Winter ~~Winter observations of~~ $ClNO_2$ formation in the region of fresh anthropogenic emissions~~polluted environments of in northern China~~: ~~Comparison~~Seasonal variability and ~~of winter and summer observations~~~~Spatiotemporal variability and~~ insights into daytime peaks in northern China

Men Xia[1], Xiang Peng[1], Weihao Wang[1,8], Chuan Yu[1,2], Zhe Wang[6], Yee Jun Tham[7], Jianmin Chen[4], Hui Chen[4], Yujing Mu[5], Chenglong Zhang[5], Pengfei Liu[5], Likun Xue[2], Xinfeng Wang[2], Jian Gao[3], Hong Li[3], and Tao Wang[1]

[1]Department of Civil and Environmental Engineering, The Hong Kong Polytechnic University, Hong Kong SAR, China
[2]Environment Research Institute, Shandong University, Ji'nan, Shandong, China
[3]Chinese Research Academy of Environmental Sciences, Beijing, China
[4]Department of Environmental Science and Engineering, Fudan University, Institute of Atmospheric Sciences, Shanghai, China
[5]Research Center for Eco-Environmental Sciences, Chinese Academy of Sciences, Beijing, China
[6]Division of Environment and Sustainability, Hong Kong University of Science and Technology, Hong Kong SAR, China
[7]Institute for Atmospheric and Earth System Research/Physics, University of Helsinki, Helsinki, Finland
[8]Hangzhou PuYu Technology Development Co., Ltd, Hangzhou, Zhejiang, China
Correspondence: Tao Wang (cetwang@polyu.edu.hk)

Abstract

Nitryl chloride ($ClNO_2$) is an important chlorine reservoir in the atmosphere that affects the oxidation of volatile organic compounds (VOCs) and the production of RO_x radicals and ozone (O_3). This study presents measurements of $ClNO_2$ and related compounds at urban, polluted rural, and polluted lower tropospheric~~mountain~~ (mountaintop) sites in the winter of 2017–2018 over the North China Plain (NCP). The nocturnal concentrations of $ClNO_2$ were lower at the urban and polluted rural sites but higher at the polluted lower tropospheric~~mountain~~ site. The winter concentrations of $ClNO_2$ were generally lower than the summer concentrations that were previously observed at these sites, which was due to the lower nitrate radical (NO_3) production rate ($P(NO_3)$) and the smaller N_2O_5 uptake coefficients ($\gamma(N_2O_5)$) in winter, despite the higher dinitrogen pentoxide (N_2O_5) to NO_3 ratios in winter. Significant daytime peaks of $ClNO_2$ were observed at all the sites during the winter campaigns, with $ClNO_2$ mixing ratios of up to 1.3 ppbv. Vertical transport of $ClNO_2$ from the residual layers and prolonged photochemical lifetime of $ClNO_2$ in winter may explain the elevated daytime concentrations. The daytime-averaged chlorine radical (Cl) production rates ($P(Cl)$) from the daytime $ClNO_2$ were 0.17, 0.11, and 0.12 ppbv h^{-1} at the polluted rural, urban, and ~~mountain~~ polluted lower tropospheric sites, respectively, which were approximately 3–4 times higher than the campaign-averaged conditions. Box model calculations showed that the Cl atoms liberated during the daytime peaks of $ClNO_2$

Formatted: Font color: Red
Formatted: Font: Times New Roman
Formatted: Font color: Red
Formatted: Font color: Red
Formatted: Font color: Red
Formatted: Font color: Red
Formatted: Font: Times New Roman
Formatted: Font color: Red
Formatted: Font color: Red

increased the RO_x levels by up to 27–37–% and increased the daily O_3 productions by up to 13–18 %. ~~These~~ Our results ~~demonstrate that~~provide new insights into the $ClNO_2$ processes in the lower troposphere impacted by fresh and intense anthropogenic emissions and reveal that~~, under polluted environments that are subject to fresh emissions, the seasonal variability of $ClNO_2$ can be explained by current knowledge, and~~ $ClNO_2$ can be an important daytime source of Cl radicals under certain conditions in winter.

Key points:

1. Winter measurements of $ClNO_2$ concentrations were made at rural, urban, and mountain sites in northern China.
2. The elevated daytime mixing ratios of $ClNO_2$ were up to 1.3 ppbv.
3. The daytime peaks of $ClNO_2$ increased the concentration of RO_x radicals by up to 27–37 % and the net O_3 production by 13–18 %.

1. Introduction

Cl is a potent atmospheric oxidant that reacts analogously to hydroxyl radicals (OH) with hydrocarbons~~ (Wang et al., 2019 b)~~(Simpson et al., 2015). Cl is highly reactive toward alkanes, with the rate constants of its reactions with alkanes being approximately 10–200 times greater than some of the OH + VOCs reactions (Atkinson and Arey, 2003; Young et al., 2014; Burkholder et al., 2015). Consequently, Cl enhances the production of RO_x (= OH + HO_2 + RO_2) via Reactions R1-R4, which promotes O_3 formation by converting nitric oxide (NO) to nitrogen dioxide (NO_2) (Reactions R3 and R5). Cl also consumes O_3 via Reaction R8. The net effect of the ~~reactivity of~~ Cl chemistry is typically the depletion of O_3 in the remote atmosphere, such as ~~in~~ the stratosphere (Molina and Rowland, 1974) and ~~over~~ remote oceans (Simpson et al., 2015; Wang et al., 2019b), and an increase in O_3 production in the polluted troposphere (Riedel et al., 2014; Xue et al., 2015).

(R1) $RH(g) + Cl(g) \rightarrow R(g) + HCl(g)$

(R2) $R(g) + O_2(g) + M \rightarrow RO_2(g) + M$

(R3) $RO_2(g) + NO(g) \rightarrow RO(g) + NO_2(g)$

(R4) $RO(g) + O_2(g) \rightarrow HO_2(g) + \text{products}$

(R5) $HO_2(g) + NO(g) \rightarrow OH(g) + NO_2(g)$

(R6) $NO_2(g) + h\nu \rightarrow NO(g) + O(^3P)$

(R7) $O_2(g) + O(^3P) + M \rightarrow O_3(g) + M$

(R8) $Cl(g) + O_3(g) \rightarrow ClO(g) + O_2(g)$

where M denotes the third body in ambient air.

Formatted: Font color: Red
Formatted: Subscript
Formatted: Font color: Red
Formatted: Font color: Red
Formatted: Font color: Red
Formatted: Subscript
Formatted: Font color: Red
Formatted: Font color: Red

The production of Cl is determined by the formation and decomposition of Cl precursors such as $ClNO_2$ (Chang et al., 2011; Simpson et al., 2015). $ClNO_2$ is produced mostly in dark conditions by the heterogeneous uptake of N_2O_5 on chloride (Cl^-)-laden aerosols (Reactions R9–R13) and undergoes photolysis during the day (Reaction R14) (Finlayson-Pitts et al., 1989). $ClNO_2$ formation is constrained by the NO_3 production rate ($P(NO_3)$, Reaction R9). NO_3 is in thermal equilibrium with N_2O_5 (Reaction R10), and the equilibrium constant (K_{eq}) depends on temperature and NO_2 concentrations. N_2O_5 formation is suppressed by NO and VOCs as they consume NO_3 (Reactions R11–12). The N_2O_5 uptake probability ($\gamma(N_2O_5)$) and $ClNO_2$ production yield ($\varphi(ClNO_2)$) are kinetic parameters with values between 0 and 1, which can be derived from the observation data of N_2O_5, $ClNO_2$, and related species (Brown et al., 2006; Phillips et al., 2016). Previous laboratory studies have demonstrated that $\gamma(N_2O_5)$ is enhanced by higher relative humidity (RH) and particulate Cl^- concentrations but suppressed by higher temperature and concentrations of aerosol nitrate (NO_3^-) and organic species (Behnke et al., 1997; Hallquist et al., 2003; Bertram et al., 2009; Griffiths and Anthony Cox, 2009).

(R9) $NO_2(g) + O_3(g) \rightarrow NO_3(g) + O_2(g)$

(R10) $NO_3(g) + NO_2(g) \leftrightarrow N_2O_5(g)$

(R11) $NO_3(g) + NO(g) \leftrightarrow 2NO_2(g)$

(R12) $NO_3(g) + VOCs(g) \rightarrow products$

(R13) $N_2O_5(g) + Cl^-(aq) \rightarrow ClNO_2(g) + NO_3^-(aq)$

(R14) $ClNO_2(g) + h\nu \rightarrow Cl(g) + NO_2(g)$

Field observations of $ClNO_2$ were first reported in the marine boundary layer off the coast of the Houston-Galveston area in the USA (Osthoff et al., 2008). Subsequent studies demonstrated the worldwide ubiquity of $ClNO_2$ and confirmed its significant role in photochemistry (Thornton et al., 2010; Mielke et al., 2011; Phillips et al., 2012; Edwards et al., 2013; Bannan et al., 2015; Wild et al., 2016; Wang et al., 2016; Bannan et al., 2019; Eger et al., 2019). The role of $ClNO_2$ in the radical budget could be more important than that of OH in winter, because OH production is reduced in winter owing to lower concentrations of O_3 and H_2O vapor in this season ~~(Haskins et al., 2019)~~. ~~Haskins et al., 2019 recently confirmed that, even when compared to OH, Cl atoms produced by $ClNO_2$ photolysis can be the dominant radical source in the early morning and during the whole day over the polluted marine boundary layer downwind of the northeast US.~~ A limited number of winter observations of $ClNO_2$ have been conducted on various platforms, including on aircrafts over northern Europe (Priestley et al., 2018) and the eastern US (Haskins et al., 2018, 2019~~9~~), on a tall tower in Boulder, USA (Riedel et al., 2013), on a mountain top in Hong Kong (Wang et al., 2016), and at ground sites in Alberta, Canada (Mielke et al., 2016) and Heshan, China (Yun et al., 2018). These studies found high $ClNO_2$ mixing ratios of up to 7.7 ppbv (Yun et al., 2018) in

Formatted: Font color: Red

winter and a contribution of $ClNO_2$ to Cl liberation of up to 83 % (Priestley et al., 2018) in urban Manchester, and that $ClNO_2$ was a more dominant radical source than OH both ~~,~~ in the early morning and the whole day in the polluted marine boundary layer downwind of the northeast US (Haskins et al., 2019). ~~In terms of the pollution level,~~ $ClNO_2$ usually exhibits higher concentrations in aged and polluted air masses than in clean air and in regions subject to significant fresh NO emissions (Wang et al., 2016; Wang et al., 2017c; Osthoff et al., 2018).

The chemical production of $ClNO_2$ in winter has some unique features compared with that in warmer seasons. Long winter nights provide more time for $ClNO_2$ production and accumulation. Lower temperatures in winter shift the N_2O_5-NO_3 equilibrium to the N_2O_5 side (Brown et al., 2003) and increase the $\gamma(N_2O_5)$ on aerosols (Bertram and Thornton, 2009). Besides, NO_x has longer lifetimes in winter compared with summer due to ~~variability in the atmospheric oxidation capacity~~less abundant OH radicals in winter and its slower reaction rate with OH (Kenagy et al., 2018). However, $P(NO_3)$ might be lower in winter due to reduced O_3 concentrations. The availability of aerosol Cl^- also varies in winter and summer. ~~The winter monsoon brings air masses from the interior of the continent, thereby suppressing the transport of sea salt to inland areas.~~ ~~However, m~~More Cl^- is emitted due to coal burning in winter (McCulloch et al., 1999; Fu et al., 2018). ~~However, i~~ In places like East Asia, ~~T~~the winter monsoon brings air masses from the interior of the continent, thereby suppressing the transport of sea salt to inland areas. ~~Thus, considering the complexity of N_2O_5 chemistry and Cl^- sources~~ Because of the contrasts in the availability of aerosol chloride and the variability in meteorology and NO_x emissions that affect the N_2O_5 chemistry, it is not clear whether $ClNO_2$ formation is more prevalent in winter.

The North China Plain (NCP) – home to Beijing and several other megacities – is one of the most industrialized and populous regions of China, and frequently suffers from severe haze pollution in winter (An et al., 2019; Fu et al., 2020). $ClNO_2$ concentrations have been measured over the NCP (Breton et al., 2018; Zhou et al., 2018), but only one study was conducted in winter (Breton et al., 2018). The present~~is~~ study presents recent field observations of $ClNO_2$ concentrations from three campaigns conducted in winter and early spring at three sites in the NCP. The results were compared with those obtained in the previous summer campaigns at the same locations. We examined the factors controlling $ClNO_2$ formation, i.e., $P(NO_3)$, the nocturnal reactivity of NO_3 and N_2O_5, $\gamma(N_2O_5)$, and $\varphi(ClNO_2)$. We then focused on the unexpected daytime peaks of $ClNO_2$ concentrations that were observed at the sites and evaluated their impact on the daytime atmospheric oxidative capacity using a chemical box model.

2. Methods

2.1 Observation sites

Field campaigns were performed in Wangdu, Beijing, and Mt. Tai in sequence during the winter-early spring of 2017 – 2018 (Table 1). The locations of the three sites are

Formatted: Subscript

Formatted: Font color: Red

Formatted: Subscript

shown in Fig. S1. The sites were selected for investigation of $ClNO_2$ in urban, rural, and mountain areas of the NCP. The winter indoor-heating period lasts from early November to 15 March of the following year (Ran et al., 2016), and thus the observations were made mostly during the heating period during which coal is intensively used. Detailed descriptions of the measurement sites are available in previous studies (Tham et al., 2016; Wang et al., 2017c; Xia et al., 2019), and a brief introduction is given here.

Table 1. Locations and periods of the field campaigns relevant to this study.

Location/ Coordinate	Site category	Season	Observation period	NO_x (ppbv)	O_3 (ppbv)
Wangdu (38.66 °N, 115.25 °E)	polluted rural	Winter[1]	9-31 December 2017	83.2 ± 81.3	4.7 ± 4.5
		Summer[2]	21 June to 9 July 2014	18.3 ± 11.8	37.8 ± 26.2
Beijing (40.04 °N, 116.42 °E)	Urban	Winter[1]	6 January to 1 February 2018	35.6 ± 37.4	14.5 ± 11.5
		Early summer[3]	24 April to 31 May 2017	22.4 ± 18.3	27.2 ± 20.6
Mt. Tai (36.25 °N, 117.10 °E)	Polluted lower troposphere	Winter to early spring[1]	7 March to 8 April 2018	2.4 ± 2.0	65.1 ± 14.1
		Summer[4]	24 July to 27 August 2014	3.1 ± 3.0	77.8 ± 20.1

~~| Location | Site category | Season | Observation period | Coordinate |~~
~~| --- | --- | --- | --- | --- |~~
~~| Wangdu | Rural | Winter[1] | 9-31 December 2017 | 38.66° N, 115.25° E |~~
~~| | | Summer[2] | 21 June to 9 July 2014 | 38.67° N, 115.20° E |~~
~~| Beijing | Urban | Winter[1] | 6 January to 1 February 2018 | 40.04° N, 116.42° E |~~
~~| | | Early summer[3] | 24 April to 31 May 2017 | |~~
~~| Mt. Tai | Mountain | Winter to early spring[1] | 7 March to 8 April 2018 | 36.25°N, 117.10°E |~~
~~| | | Summer[4] | 24 July to 27 August 2014 | |~~

[1]Observations from this study.
[2-4]Observations from previous studies, i.e., Tham et al. (2016), Xia et al. (2019), and Wang et al. (2017c), respectively.

Our observations at the Wangdu site were part of the Campaign of Oxidation Potential Research for air Pollution in winter (COPPER). The Wangdu site is located in Dongbaituo Village, Hebei Province. Local villagers use coal stoves for cooking and

Formatted Table
Formatted: Subscript
Formatted: Subscript
Formatted: Superscript
Formatted: Superscript
Formatted: Superscript
Formatted: Superscript
Formatted: Superscript
Formatted: Superscript
Formatted: Centered

heating during winter. National road G4 and provincial road S335 are 1 km and 3 km to the west of the sampling site, respectively. Many heavy-duty trucks passed through G4 and S335 every night during the study period, emitting a large amount of NO_x and particulate matters. Therefore, the site experienced heavy pollution from coal burning and road traffic (Peng et al., 2020).

The Beijing site is located at the Chinese Research Academy of Environmental Science (CRAES), which is 15 km northeast of the city center. The sampling site is surrounded by intra-city roads, commercial buildings, and residential buildings with few industrial facilities. When the prevailing wind originates from the north (i.e., remote mountainous regions), the site is upwind from the Beijing downtown area and thus is less polluted. However, when the wind originates from the south, the site receives pollutants from Beijing's urban areas in the NCP (Xia et al., 2019).

Mt. Tai is located approximately 40 km south of Jinan City (population: 8.9 million) and 15 km north of Tai'an City (population: 5.6 million) (Wen et al., 2018). Measurements were taken at Mt. Tai meteorological station (1534 m a.s.l.). The site is isolated from the anthropogenic emissions of tourist areas and is not affected by local emissions. The observation period, i.e., March to April, was in early spring in the NCP. However, considering the low temperature (4.6 ± 6.3 °C~~°C~~) observed on top of Mt. Tai, this study considered the observation period as winter to early spring.

2.2 Measurements of N_2O_5 and $ClNO_2$ concentrations

N_2O_5 and $ClNO_2$ were simultaneously measured by a chemical ionization mass spectrometer with a quadrupole mass analyzer (Q-CIMS; THS Instruments). The principles and calibrations of the Q-CIMS measurements are available in previous studies (Wang et al., 2016; Tham et al., 2016; Wang et al., 2017c; Xia et al., 2019). Briefly, ~~T~~the primary ions used in the Q-CIMS were iodide (I^-) and its water clusters, which were generated using CH_3I with an inline ionizer (^{210}Po). The iodide adducts, namely $IN_2O_5^-$ and $ICINO_2^-$, were then detected by the mass spectrometer. An example of the mass spectrum is shown in Fig. S2. The integration time of the signals recorded by the Q-CIMS is shown in Table S1. The isotopic ratios of $I^{35}ClNO_2^-$ and $I^{37}ClNO_2^-$ in the ambient data were used to confirm the identity of $ClNO_2$ (Fig. S3). Gas-phase mixtures of NO_2 and O_3 produced N_2O_5 ~~in a dynamic gas calibrator (Sabio Instruments)~~ for N_2O_5 calibration. The synthetic N_2O_5 was converted to $ClNO_2$ by passage through a humidified NaCl slurry for $ClNO_2$ calibration. ~~Multi-concentration calibrations of N_2O_5 and $ClNO_2$ were performed once in the Mt. Tai campaign (Fig. SX).~~ The dependence of the N_2O_5 sensitivities ~~(normalized to the signal of $I(H_2O)^-$)~~ on ambient RH was tested once in each campaign and used to calibrate the N_2O_5 data (Fig. S4a). $ClNO_2$ sensitivities were found not affected by RH (Fig. S4b). Single-concentration~~On-site~~ calibrations of N_2O_5 and $ClNO_2$ were performed every 1 – 2 days, which showed stable sensitivities of N_2O_5 and $ClNO_2$ (Text S1, and Fig. S5~~X~~). And ~~–~~the linearity of the N_2O_5 and $ClNO_2$ signals to concentrations was checked via ~~M~~multi-concentration

Formatted: Font color: Red
Formatted: Not Highlight
Formatted: Font color: Red
Formatted: Font color: Red, Subscript
Formatted: Font color: Red
Formatted: Font color: Red, Not Highlight
Formatted: Font color: Red
Formatted: Font color: Red, Not Highlight
Formatted: Not Highlight
Formatted: Font color: Red
Formatted: Font color: Red, Not Highlight
Formatted: Font color: Red
Formatted: Font color: Red, Not Highlight
Formatted: Font color: Red
Formatted: Font color: Red, Not Highlight
Formatted: Not Highlight
Formatted: Font color: Red, Not Highlight
Formatted: Not Highlight
Formatted: Font color: Red, Not Highlight

calibrationss ~~of N_2O_5 and $ClNO_2$ were performed once~~ in the Mt. Tai campaign (Fig. S~~X~~)6). ~~The dependence of the N_2O_5 sensitivities (normalized to the signal of $I(H_2O)^-$) on ambient RH was tested and used to calibrate the N_2O_5 data (Fig. S4),~~ and ~~, the normalized sensitivity of N_2O_5 was determined as the signal ratio of $I(N_2O_5)^-$ to $I(H_2O)^-$ in the presence of 1 pptv of N_2O_5. The normalized sensitivities of N_2O_5 and $ClNO_2$ were (1.3–2.2) × 10^{-5} Hz/Hz/pptv and (0.9–1.8) × 10^{-5} Hz/Hz/pptv, respectively during the three campaigns. The detection limits of N_2O_5 and $ClNO_2$ were 6.9–7.3 pptv and 3.8–5.3 pptv (3σ in 5 minutes), respectively,~~ and ~~B~~backgrounds ~~detections~~ of N_2O_5 and $ClNO_2$ were ~~conducted~~ determined ~~every day~~ by passing the ambient air through glass wool once a day at different time. The background signals of N_2O_5 (3.3 – 7.7 pptv~~(xx+-xx)~~ and $ClNO_2$ (1.0 – 7.5 pptv~~xx+-xx~~) were stable~~,~~ and independent of the ~~constant at different~~ time of the day (Fig. S7~~X~~). The detection limits of N_2O_5 and $ClNO_2$ were 6.9 – 7.3 pptv and 3.8 – 5.3 pptv, which is defined here as three times of the standard deviation of the background signals ~~(3σ in 5 minutes)~~ ~~, respectively~~ (Table~~s~~ S2~~X~~). ~~and largely lower than their ambient signals. The dependence of the N_2O_5 sensitivities (normalized to the signal of $I(H_2O)^-$) on ambient RH was tested and used to calibrate the N_2O_5 data (Fig. S4). The normalized sensitivity of N_2O_5 is the signal ratio of $I(N_2O_5)^-$ to $I(H_2O)^-$ in the presence of 1 pptv of N_2O_5. The normalized sensitivities and detection limits of the N_2O_5 and $ClNO_2$ measurements were (0.9–2.2) × 10^{-5} Hz/Hz/pptv and 4–7 pptv (3σ in 5 minutes), respectively during the three campaigns. The normalized sensitivities of N_2O_5 and $ClNO_2$ were (1.3–2.2) × 10^{-5} Hz/Hz/pptv and (0.9–1.8) × 10^{-5} Hz/Hz/pptv, respectively during the three campaigns. The detection limits of N_2O_5 and $ClNO_2$ were 6.9–7.3 pptv and 3.8–5.3 pptv (3σ in 5 minutes), respectively. The variation in the sensitivities and detection limits of N_2O_5 and $ClNO_2$ were small within each campaign (Text S1, Table S1, and Fig. S5).~~ A virtual-impactor design (Peng et al., 2020) was adopted, and the sampling tube was replaced daily to minimize inlet artifacts.

2.3 Other measurements

The trace gases, particle number size distribution (PNSD), ionic composition of aerosols and other species were simultaneously measured (Table S3~~2~~). Online ~~VOCs~~ non-methane hydrocarbons ~~measurements~~ were ~~performed~~ measured by gas chromatography-flame-ionization detection/mass spectrometry (GC-FID/MS; Chromatotec Group) at the Beijing site (Zhang et al., 2017) and Wangdu site (Zhang et al., 2020). At Mt. Tai, we used canisters to collect air samples, which were analyzed using GC-FID/MS. In Wangdu and Mt. Tai, oxygenated volatile organic compounds (OVOCs) samples were collected on DNPH-coated sorbent cartridges followed by post-campaign analysis using high performance liquid chromatography. The ionic compositions of $PM_{2.5}$ (e.g., NH_4^+, NO_3^-, SO_4^{2-}, and Cl^-) were quantified by the Monitor for AeRosols and GAses in ambient air (MARGA, Metrohm) at the Beijing and Mt. Tai sites (Wen et al., 2018). An aerosol chemical speciation monitor (ACSM, Aerodyne Research Inc.) was utilized at the Wangdu site to monitor the non-refractory components of these ions in $PM_{2.5}$. The concentrations of the NO_3^-, SO_4^{2-}, and NH_4^+ measured simultaneously by the MARGA and ACSM were in good agreement, whereas

Formatted: Not Highlight
Formatted: Not Highlight
Formatted: Font: (Default) Times New Roman, 12 pt
Formatted: Font: (Default) Times New Roman, 12 pt
Formatted: Font: (Default) Times New Roman, 12 pt
Formatted: Not Highlight
Formatted: Not Highlight
Formatted: Not Highlight
Formatted: Not Highlight
Formatted: Not Highlight
Formatted: Not Highlight

the concentration of Cl^- measured by the ACSM was slightly lower than that measured by the MARGA, which was possibly due to the significant proportion of refractory chloride, e.g., NaCl, present in the aerosols (Xia et al., 2020). We assumed that the particles sampled by a wide-range particle spectrometer (WPS) were spherical in shape and calculated the aerosol surface area density (S_a) and volume density (V_a). A parameterization was adopted to consider the hygroscopic growth factor (GF) of aerosol sizes, as follows: $GF = a \times \left(b+\frac{1}{1-RH}\right)^{1/3}$ (Lewis, 2008), where the parameters a and b were derived as 0.582 and 8.460, respectively in a previous field study over the NCP (Achtert et al., 2009).

2.4 Calculation of N_2O_5 loss and $ClNO_2$ production

Some analytical metrics were ~~estimated~~ calculated from the observation data. $P(NO_3)$ was calculated using Eq. (1), where k_1 represents the rate constant of Reaction R9 (Atkinson and Lloyd, 1984).

(Eq. 1) $P(NO_3) = k_1 \times [O_3] \times [NO_2]$

$k(NO_3)$ during the night was calculated~~estimated~~ using the measured mixing ratios of NO and ~~VOCs which include~~ non-methane hydrocarbons that ~~can be~~were measured by GC (section 2.3). ~~Due to the challenge of obtaining a full suite of VOCs~~As most OVOCs react with NO_3 ~~reactions~~ at much slower rates compared to those with hydrocarbons especially alkenes (Atkinson and Arey, 2003), the OVOCs~~hey~~ were not included in the calculation of $k(NO_3)$. Nonetheless~~,~~, the $k(NO_3)$ ~~might~~might be slightly underestimated here.

(Eq. 2) $k(NO_3) = \sum k_i[VOC_i] + k_{NO+NO_3}[NO]$

where k_i is the rate constant for a specific VOC + NO_3 reaction and is adopted from ~~(~~Atkinson and Arey (~~,~~2003) and k_{NO+NO_3} represents the rate constant for Reaction R11 (DeMore et al., 1997). The ambient concentrations of NO_3 were estimated by assuming that NO_3 and N_2O_5 were in dynamic equilibrium (DeMore et al., 1997).

(Eq. 3) $[NO_3] = \frac{[N_2O_5]}{[NO_2]K_{eq}}$

The loss rates of NO_3 due to NO and VOCs were then calculated by $k_{NO+NO_3}[NO][NO_3]$ and ~~$\sum\sum k_i[VOC_i][NO_3]$~~, respectively.

The loss rate coefficient of N_2O_5 on the aerosol surface ($k(N_2O_5)$) is expressed as follows.

(Eq. 4) $k(N_2O_5) = 0.25 \times c(N_2O_5) \times S_a \times \gamma(N_2O_5)$

where $c(N_2O_5)$ represents the average molecular velocity of N_2O_5. The rate constants (k_1, k_i, and k_{NO+NO_3}) and equilibrium constant (K_{eq}) are calculated as temperature-dependent parameters.

Formatted: Font: Times New Roman
Formatted: Font: Times New Roman
Formatted: Font: Times New Roman
Formatted: Font: (Default) Times New Roman, 12 pt
Formatted: Font color: Red
Formatted: Font color: Red, Not Highlight
Formatted: Font color: Red, Subscript, Not Highlight
Formatted: Font color: Red, Not Highlight
Formatted: Font: Italic, Font color: Red, Not Highlight
Formatted: Font color: Red, Not Highlight
Formatted: Font color: Red, Subscript, Not Highlight
Formatted: Font color: Red, Not Highlight
Formatted: Font color: Red, Not Highlight
Formatted: Font color: Red
Formatted: Font color: Red, Not Highlight
Formatted: Font color: Red
Formatted: Font: Times New Roman
Formatted: Font: Times New Roman
Formatted: Font: Times New Roman
Formatted: Font: Times New Roman

$\gamma(N_2O_5)$ and $\varphi(ClNO_2)$ were estimated using steady-state analysis in applicable cases (Brown et al., 2006). This method assumes a steady state of N_2O_5, which means that the production rate of N_2O_5 is equal to its loss rate. We adopted the criteria described by Xia et al. (2020) to select the cases, namely low concentrations of NO, an increasing trend of $ClNO_2$ concentrations, and stable air masses. Equation (5) was then established by plotting $\tau(N_2O_5)^{-1} \times [NO_2] \times K_{eq}$ against $0.25 \times S_a \times C_{N_2O_5} \times [NO_2] \times K_{eq}$, with $\gamma(N_2O_5)$ as the slope and $k(NO_3)$ as the intercept in the linear regression (Brown et al., 2003). Here, the derived $\gamma(N_2O_5)$ was accepted when the regression had $R^2 > 0.5$ and $k(NO_3) > 0$.

(Eq. 5) $\tau(N_2O_5)^{-1} \times K_{eq} \times [NO_2] \approx 0.25 \times C_{N_2O_5} \times S_a \times K_{eq} \times [NO_2] \times \gamma(N_2O_5) + k(NO_3)$

$\varphi(ClNO_2)$ was then calculated using the following equation:

(Eq. 6) $$\varphi(ClNO_2) = \frac{d[ClNO_2]/dt}{k(N_2O_5)[N_2O_5]}$$

where $d[ClNO_2]/dt$ and $[N_2O_5]$ represent the increasing rate of $ClNO_2$ production and the average concentration of N_2O_5, respectively within the selected cases.

2.5 Box model

An observation-based chemical box model was utilized to simulate the concentrations of Cl and RO_x radicals and the production and loss pathways of O_3. The detailed model description is available in Peng et al. (2020). Based on Master Chemical Mechanism (MCM) v3.3.1 (Jenkin et al., 2015), Peng et al. (2020) modified the chemical mechanisms to include up-to-date gas-phase chlorine and bromine chemistry. The observed N_2O_5, $ClNO_2$, NO_x, HONO, O_3, jNO_2, and related species were constrained in the model for every 10 minutes of model time, after interpolating or averaging the data (Table S43). The mixing ratios of NMHCs and ~~oxygenated volatile organic compounds (~~OVOCs~~) and VOCs~~ (Section 2.3) were constrained every hour. As OVOCs were not measured in Beijing in this study, we adopted the concentrations of OVOCs measured in~~a~~ previous studies~~y~~ in winter Beijing (Gu et al., 2019; Qian et al., 2019)~~(Tan et al., 2018)~~. We also assumed the ~~the~~ CH_4 mixing ratio ~~of CH_4 to be constant at~~to be~~of~~ 2000 ppbv, which was the mean value in~~for~~ summer at ~~in~~ Wangdu ~~and Beijing~~ (Tan et al., 2017), for our Wangdu and Beijing sites. We acknowledge that the adoption of the summer CH_4 concentrations for our winter studies~~y~~ may underestimate the CH_4 level, but the effect on the RO_x budget is expected to be insignificant due to much smaller contribution of CH_4 to RO_x than NMHCs and OVOCs in polluted environments. ~~As Wangdu and Beijing are closer to fresh emission sources compared with Mt. Tai, the CH_4 concentrations may be underestimated in Wangdu and Beijing and cause slight uncertainties to the RO_x budgets.~~ The photolysis frequencies of $ClNO_2$, O_3, and other species were simulated according to the solar zenith angle using the Tropospheric Ultraviolet and Visible (TUV) Radiation model and scaled by the observed jNO_2 values. Numerical experiments were conducted by constraining (Case 1) and not constraining $ClNO_2$ data (Case 2) at each site. The differences in the radical concentrations and O_3 budgets between Cases 1 and 2 represented the effect of $ClNO_2$.

Formatted ... [1]
Formatted ... [2]
Formatted ... [3]
Formatted ... [4]
Formatted ... [5]

For example, the increase in RO_x (%) due to $ClNO_2$ was calculated by (RO_x_w – RO_x_wo) / RO_x_wo, where RO_x_w represents the concentration of RO_x in Case 1 with $ClNO_2$ constrained in the model and RO_x_wo represents the concentration of RO_x in Case 2 without $ClNO_2$ constrained.

3. Results

3.1 Overall measurements, diurnal patterns and comparison with other studies

The time series of N_2O_5 and $ClNO_2$ levels in the three campaigns are displayed in Fig. 1. Overall, elevated levels of N_2O_5 and $ClNO_2$ were observed with different patterns at each site. The ground sites (Wangdu and Beijing) were characterized by high NO_x levels (83.2 ± 81.3 ppbv and 35.6 ± 27.3 ppbv, respectively) and low O_3 levels (8.5 ± 8.8 ppbv and 17.3 ± 11.4 ppbv, respectively), whereas the mountain site, Mt. Tai, was marked by relatively lower NO_x levels (2.4 ± 2.0 ppbv) and higher O_3 levels (64.6 ± 14.7 ppbv) (Fig. S8~~6~~). The campaign-averaged mixing ratios of $ClNO_2$ were similar at the ground sites (71 ± 132 pptv and 76 ± 103 pptv in Wangdu and Beijing, respectively), and were significantly lower than that at Mt. Tai (179 ± 247 pptv). The nocturnal ratio of $ClNO_2/N_2O_5$ at each site displayed large day-to-day variability, which was positively dependent on the ambient RH (Fig. S9~~7~~) and, to a lesser extent, positively correlated with S_a (figure not shown).

Formatted: Font color: Red

Formatted: Font color: Red

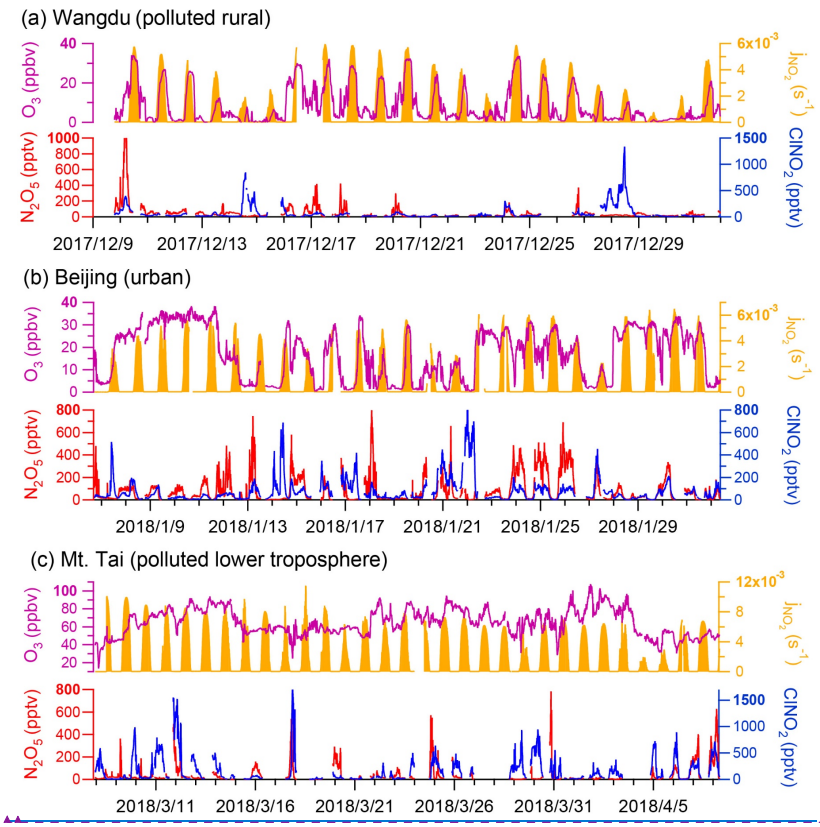

368

Formatted: Font: Times New Roman

Formatted: Font: Times New Roman

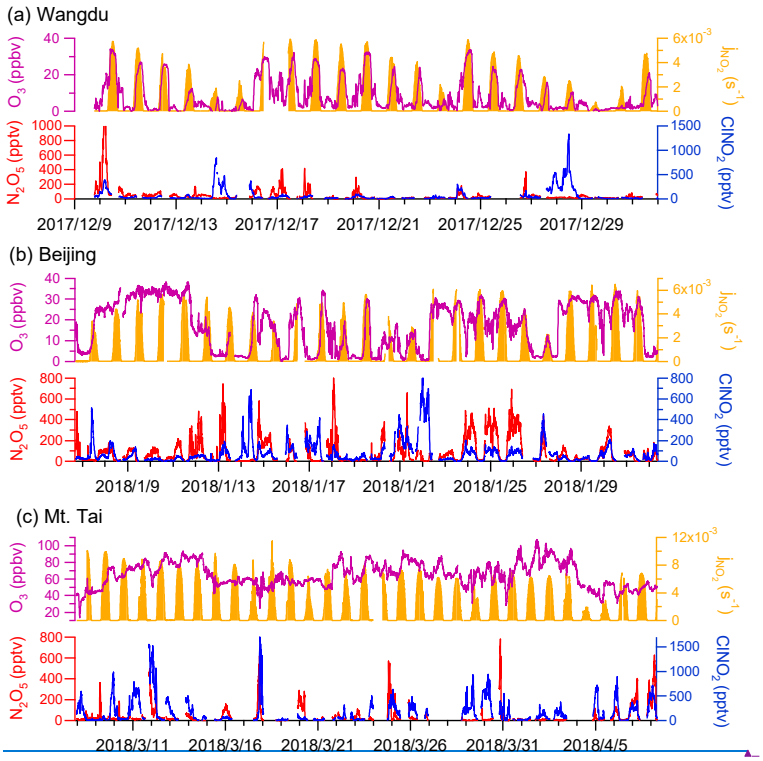

Figure 1. Overall observations of N_2O_5, $ClNO_2$ and related species at the **(a)** Wangdu, **(b)** Beijing, and **(c)** Mt. Tai sites.

The campaign-averaged diurnal patterns of the mixing ratios of N_2O_5, $ClNO_2$, and related species are depicted in Fig. 2. $ClNO_2$ levels typically exhibited a daily cycle, peaking at night and decreasing during the day. The diurnal pattern of $ClNO_2$ at the Wangdu site in winter was an exception, with elevated concentrations (10–90 percentiles) around midday (12:00–14:00 local time; LT), which resulted from a noontime peak in $ClNO_2$ concentrations during a few days at Wangdu. The detailed observation results from each site are separately introduced as follows.

Formatted: English (Hong Kong SAR)

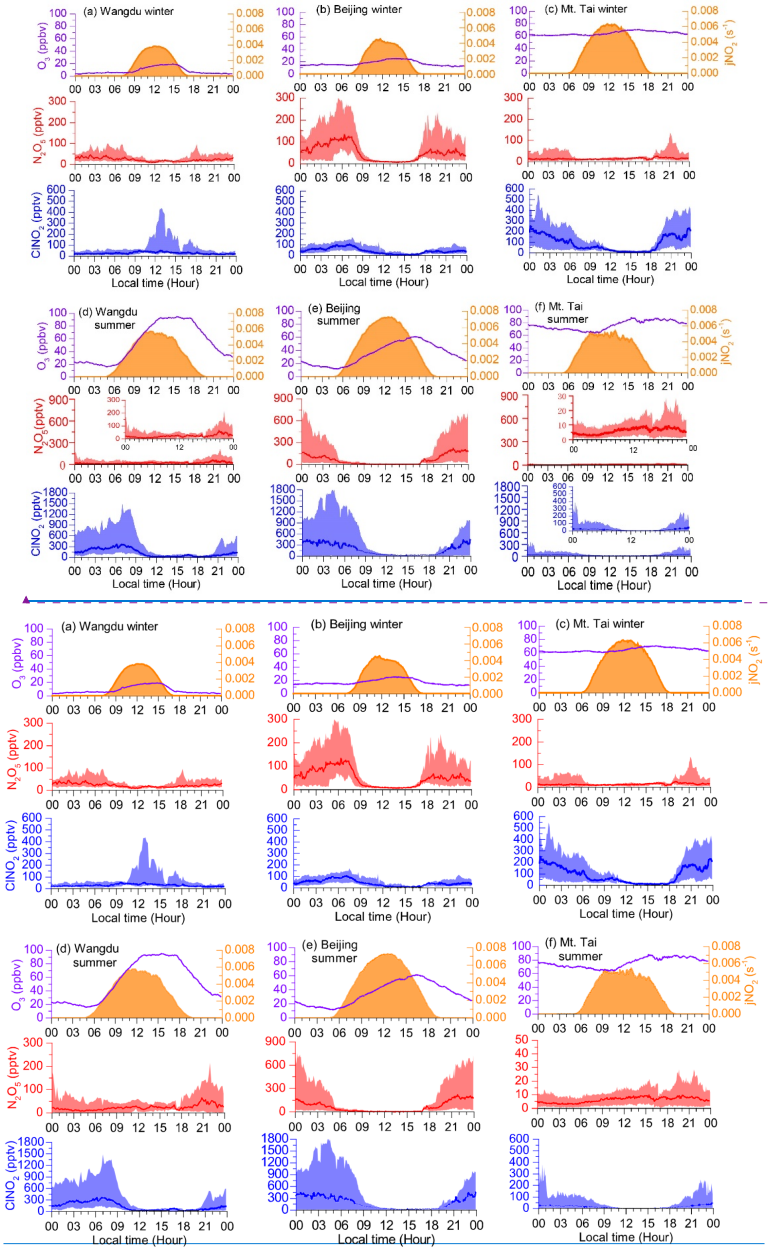

Figure 2. Diurnal average levels of N_2O_5, $ClNO_2$, O_3, and jNO_2 observed at the Wangdu, Beijing, and Mt. Tai sites throughout the campaign in winter (this study) and previous summer field studies (Table 1). The shaded areas indicate the 10th and 90th percentiles.

Formatted: Font: Times New Roman

The nocturnal production of $ClNO_2$ was insignificant in Wangdu despite the presence of abundant Cl^- (3.3 ± 3.2 μg m^{-3} throughout the observation), which likely originated from the intensive residential coal combustion in the area (Peng et al., 2020). The Wangdu site experienced high mass concentrations of $PM_{2.5}$ (a maximum of approximately 450 μg m^{-3}) and very large mixing ratios of NO (a maximum of approximately 350 ppbv). The wind rose analysis showed that the high concentrations of NO originated from the west of the sampling site where two major roads were located. Numerous heavy-duty trucks on these roads were responsible for high NO concentrations. The presence of abundant NO inhibited N_2O_5 formation by consuming O_3 and NO_3 at the Wangdu site. When the ambient concentrations of NO substantially decreased, e.g., on 10 December, the N_2O_5 mixing ratios increased to 1 ppbv. The mixing ratios of $ClNO_2$ were mostly low (< 200 pptv) during the night. The relationship between nighttime levels of $ClNO_2$ and grouped NO and NO_x concentrations is shown in Fig. 3. $ClNO_2$ showed higher levels when the NO mixing ratios were below 10 ppbv and NO_x mixing ratios ranged 10 ~ 20 ppbv (Fig. 3a, d). However, significant daytime peaks in $ClNO_2$ mixing ratios were observed on 14 and 28 December, reaching approximately 0.8 ppbv and 1.3 ppbv, respectively. The daytime peaks in $ClNO_2$ concentrations at the three sites are discussed in detail in Section 3.3. For comparison, the ambient mixing ratios of NO in the summer campaign at Wangdu were much lower (mostly 0-10 ppbv) and O_3 mixing ratios were much higher (i.e., exceeded 90 ppbv on most days), which favored the production of N_2O_5 and $ClNO_2$ (Tham et al., 2016).

Formatted: Subscript

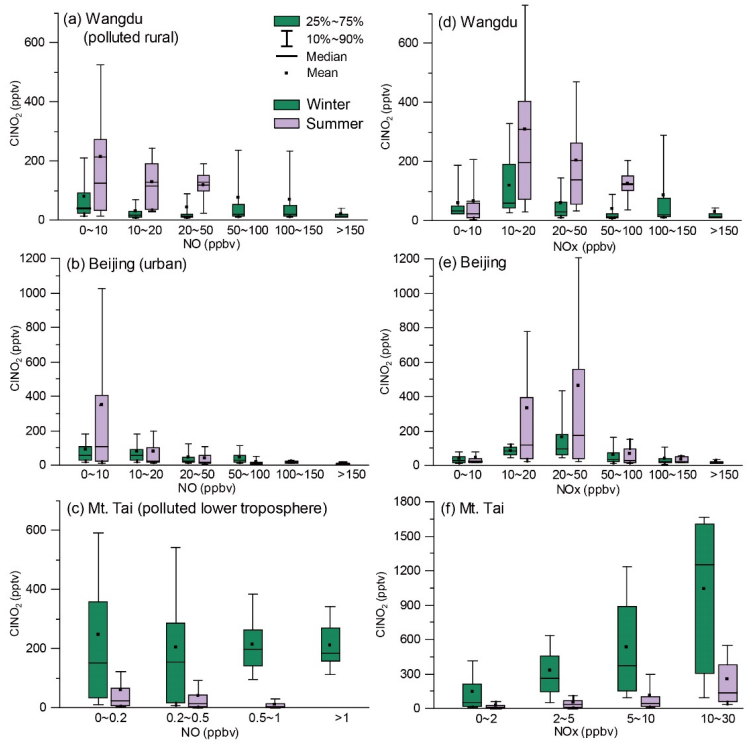

Figure 3. The relationship between nighttime levels of $ClNO_2$ and grouped NO (a, b, and c) and NO_x (d, e, and f) mixing ratios in the winter (green color) and summer (purple color) campaigns. The difference in the scale of $ClNO_2$ in Fig. 3c and Fig. 3f is caused by statistic factors, since only 10th to 90th percentile of $ClNO_2$ data is shown here.

The winter Beijing observations showed that there was significant production of N_2O_5 but limited conversion of N_2O_5 to $ClNO_2$ in dry conditions. The observation period in Beijing was divided into polluted days (24-h $PM_{2.5} > 75$ μg m^{-3}; China's Grade II air quality standard for $PM_{2.5}$) and clean days (24-h $PM_{2.5} < 35$ μg m^{-3}; Grade I standard). The polluted periods were characterized by simultaneous high levels of $PM_{2.5}$ and NO, e.g., on 19 January. The clean periods were marked by relatively high mixing ratios of O_3, low levels of $PM_{2.5}$ and NO_x, e.g., from 8 to 11 January. Both polluted and clean conditions were unfavorable for $ClNO_2$ formation owing to the high concentrations of NO on the polluted days and the low concentrations of NO_2 and aerosols on the clean days. Moreover, the RH observed in Beijing was typically below 40 %, which indicated relatively slow heterogeneous loss of N_2O_5 and slow $ClNO_2$ formation. Consequently, N_2O_5 mixing ratios frequently accumulated to elevated levels, exceeding 0.4 ppbv on 10 of the 26 observation nights, and the mixing ratio of $ClNO_2$ was mostly below 0.4 ppbv. Nighttime levels of $ClNO_2$ in winter Beijing were higher

Formatted: Font: Times New Roman
Formatted: Centered, Indent: First line: 0 ch
Formatted: Font color: Red
Formatted: Font color: Red, Subscript

when NO mixing ratios ranged 0 ~ 10 ppbv and NO_x mixing ratios ranged 20 ~ 50 ppbv (Fig. 3b, d). The highest mixing ratios of $ClNO_2$ were observed (up to approximately 0.8 ppbv) when the site occasionally intercepted air masses with a higher RH (approximately 75 %), e.g., on the night of 22 January. This result is similar to the previous observation in Beijing (Xia et al., 2019), in which the ratio of $ClNO_2$ to N_2O_5 increased significantly from late spring with a low RH (10 – 30 %) to early summer with a higher RH (20 – 80 %). The overall mixing ratios of $ClNO_2$ in the present Beijing study in winter were also significantly lower than those reported in summer (maximum of 1.4 ppbv to 2.9 ppbv) in other studies (Breton et al., 2018; Zhou et al., 2018).

Elevated mixing ratios of $ClNO_2$ (i.e., above 0.5 ppbv) were frequently recorded at the Mt. Tai station in winter. Nighttime levels of $ClNO_2$ were slightly higher when NO levels were below 0.5 ppbv (Fig. 3c) and showed a positive correlation with NO_x levels (Fig. 3f). High concentrations of $PM_{2.5}$ (34.5 ± 27.3 μg m^{-3}) and high RH (63.6 ± 27.1 %) favored the $ClNO_2$ formation at Mt. Tai. The maximum level of $ClNO_2$ (approximately 1.7 ppbv) was observed just before midnight on 18 March, which was slightly lower than the highest concentration observed at Mt. Tai in the summer of 2014 (Wang et al., 2017c). The elevated concentrations of $ClNO_2$ observed in the previous summer study at Mt. Tai were due to emissions from distinct coal-fired power plants, whereas this winter study found that coal burning had less effect on concentrations of $ClNO_2$. The campaign-averaged levels of SO_2 and particulate SO_4^{2-} were 1.6 ± 1.6 ppbv and 3.6 ± 2.9 μg m^{-3}, respectively, during the winter observations, which were significantly lower than those observed in the summer campaigns (2.9 ± 3.7 ppbv and 14.8 ± 9.0 μg m^{-3}, respectively). The decreases in SO_2 and sulfate were attributed to ~~The reduced~~ strengthened emission control for ~~effect from~~ coal-fired power generation ~~causedwas due to the continued decrease in SO_2 emissions~~ during 2014 – 2018 and also less transport of emissions from the ground to the Mt. Tai site (1534 m a.s.l.) in late winter and early spring compared with that in summer.

We compared the observed winter concentrations of $ClNO_2$ with those reported in previous studies in Asia, North America, and Europe (Fig. ~~4~~3). The highest winter concentrations of $ClNO_2$ to date were observed in southern China, with a maximum level of 4.7 ppbv at a mountain top in Hong Kong in aged urban/industrial plumes from the Pearl River Delta (PRD) (Wang et al., 2016) and 8.3 ppbv during a severe pollution episode within the PRD (Yun et al., 2018). The high-concentration $ClNO_2$ events in southern China were due to concurrent high levels of $PM_{2.5}$ and O_3 (e.g., 400 μg m^{-3} and 160 ppbv found by Yun et al., 2018), which contrasts the high concentrations of $PM_{2.5}$ and low concentrations of O_3 over northern China during the cold winter. The winter mixing ratios of $ClNO_2$ in the US and Europe range from approximately 0.3 ppbv in urban California (Mielke et al., 2016) and urban Manchester (Priestley et al., 2018), respectively, to 1.3 ppbv in the outflow of coastal urban areas (Riedel et al., 2013; Haskins et al., 2019). In general, the winter concentrations of $ClNO_2$ over northern China were comparable to or slightly higher than those observed in the US and Europe.

Formatted: Subscript
Formatted: Font color: Red
Formatted: Font color: Red
Formatted: Font color: Red
Formatted: Font color: Red
Formatted: Not Highlight
Formatted: Subscript, Not Highlight
Formatted: Not Highlight
Formatted: Font color: Red
Formatted: Subscript
Formatted: Font color: Red
Formatted: Font color: Red

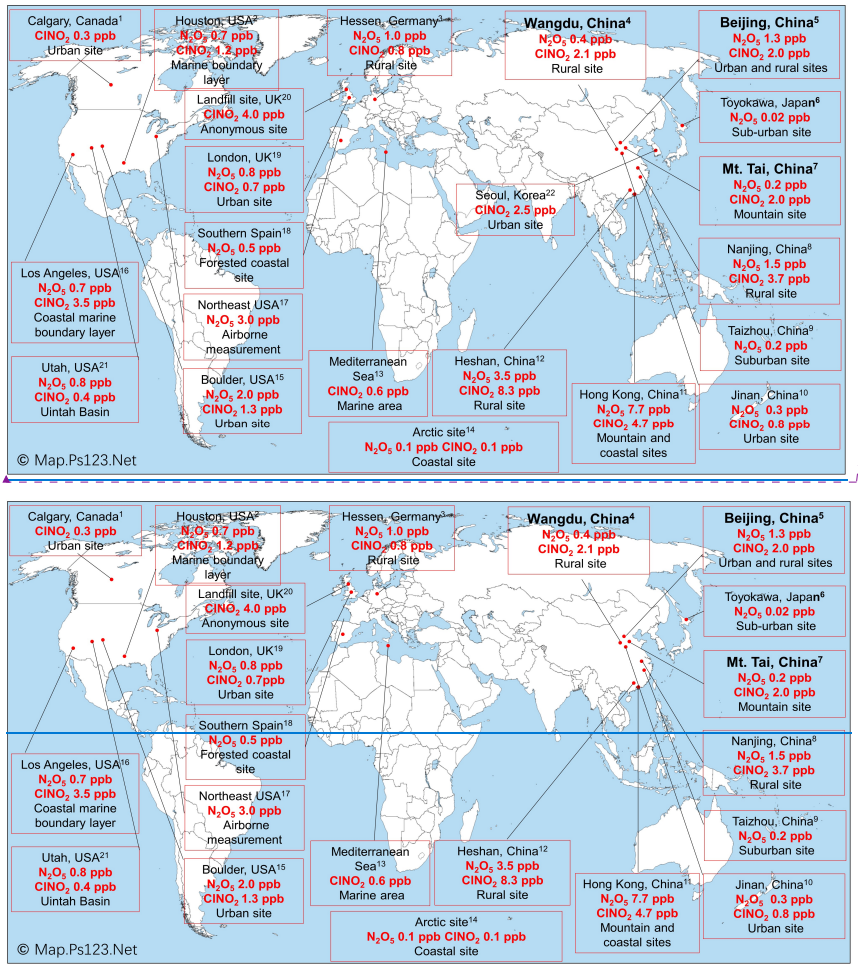

Calgary, Canada[1]
ClNO2 0.3 ppb
Urban site
Houston, USA[2]
N2O5 0.7 ppb
ClNO2 1.2 ppb
Marine boundary layer
Hessen, Germany[3]
N2O5 1.0 ppb
ClNO2 0.8 ppb
Rural site
Wangdu, China[4]
N2O5 0.4 ppb
ClNO2 2.1 ppb
Rural site
Beijing, China[5]
N2O5 1.3 ppb
ClNO2 2.0 ppb
Urban and rural sites
Landfill site, UK[20]
ClNO2 4.0 ppb
Anonymous site
Toyokawa, Japan[6]
N2O5 0.02 ppb
Sub-urban site
London, UK[19]
N2O5 0.8 ppb
ClNO2 0.7ppb
Urban site
Mt. Tai, China[7]
N2O5 0.2 ppb
ClNO2 2.0 ppb
Mountain site
Southern Spain[18]
N2O5 0.5 ppb
Forested coastal site
Nanjing, China[8]
N2O5 1.5 ppb
ClNO2 3.7 ppb
Rural site
Los Angeles, USA[16]
N2O5 0.7 ppb
ClNO2 3.5 ppb
Coastal marine boundary layer
Northeast USA[17]
N2O5 3.0 ppb
Airborne measurement
Taizhou, China[9]
N2O5 0.2 ppb
Suburban site
Utah, USA[21]
N2O5 0.8 ppb
ClNO2 0.4 ppb
Uintah Basin
Boulder, USA[15]
N2O5 2.0 ppb
ClNO2 1.3 ppb
Urban site
Mediterranean Sea[13]
ClNO2 0.6 ppb
Marine area
Heshan, China[12]
N2O5 3.5 ppb
ClNO2 8.3 ppb
Rural site
Hong Kong, China[11]
N2O5 7.7 ppb
ClNO2 4.7 ppb
Mountain and coastal sites
Jinan, China[10]
N2O5 0.3 ppb
ClNO2 0.8 ppb
Urban site
Arctic site[14]
N2O5 0.1 ppb ClNO2 0.1 ppb
Coastal site
© Map.Ps123.Net

Figure 43. Previous observations of $ClNO_2$ and N_2O_5 levels worldwide. Observation sites in this study are shown in bold. The $ClNO_2$ and N_2O_5 levels shown are the highest that were measured at these sites. Footnotes associated with the locations refer to the references as follows. 1. (Mielke et al., 2011; Mielke et al., 2016; Osthoff et al., 2018). 2. (Osthoff et al., 2008; Faxon et al., 2015). 3. (Phillips et al., 2012). 4. (Tham et al., 2016; Liu et al., 2017). 5. (Wang et al., 2017a; Breton et al., 2018; Wang et al., 2018; Zhou et al., 2018; Xia et al., 2019). 6. (Nakayama et al., 2008). 7. (Wang et al., 2017c). 8. (Xia et al., 2020). 9. (Wang et al., 2019a). 10. (Wang et al., 2017b). 11. (Wang et al., 2016; Yun et al., 2017; Yan et al., 2019). 12. (Yun et al., 2018). 13. (Eger et al., 2019). 14. (Apodaca et al., 2008; McNamara et al., 2019). 15. (Thornton et al., 2010; Riedel et al., 2013). 16. (Riedel et al., 2012; Mielke et al., 2013). 17. (Brown et al., 2006; Brown et al., 2007; Haskins et al., 2018). 18. (Crowley et al., 2011). 19. (Bannan et al., 2015; Sommariva et al., 2018). 20. (Bannan et al., 2019). 21. (Edwards et al., 2013;

Formatted: Font: Times New Roman

Formatted: Font: Bold

Formatted: Font color: Red

Formatted: Font color: Red

Wild et al., 2016; McDuffie et al., 2019). 22. (Jeong et al., 2019).

3.2 NO_3 production and loss pathways

To gain insight into the processes controlling the variability in concentrations of $ClNO_2$, nocturnal $P(NO_3)$ and NO_3 loss pathways were compared using Eqs. (1-5) in Section 2.4. The average $P(NO_3)$ was comparable at the three sites in winter, ranging from 0.15 ppbv h^{-1} to 0.25 ppbv h^{-1}, and these rates were significantly lower than the respective summer values (Fig. 54a). The lower $P(NO_3)$ in winter was caused by both lower k_1 and lower $[NO_2] \times [O_3]$ in winter (see Eq. 1). The lower k_1 in winter is caused by lower temperature in winter, while the lower $[NO_2] \times [O_3]$ in winter is mainly caused by less photochemical production of O_3 and more NO that consumes the available O_3 in winter (Table S56). Nighttime NO_3 removal through NO_3 and N_2O_5 was estimated by comparing $k(NO_3) \times [NO_3]$ (Eqs. 2–3) and $k(N_2O_5) \times [N_2O_5]$ (Eqs. 4–5). The average $\gamma(N_2O_5)$ values derived from each campaign (Table S654 and Fig. S108) were used in Eq. (4). The nighttime NO_3 loss via NO titration and VOC oxidation was greater than the N_2O_5 heterogeneous loss in all the winter and summer campaigns (Fig. 54b). These were the campaign average results. In contrast, the N_2O_5 loss was greater than the NO_3 loss in selected cases in summer at Mt. Tai (Wang et al., 2017c). To determine the nocturnal loss of NO_3, we further compared the N_2O_5/NO_3 ratio and $\gamma(N_2O_5)$ at the three sites.

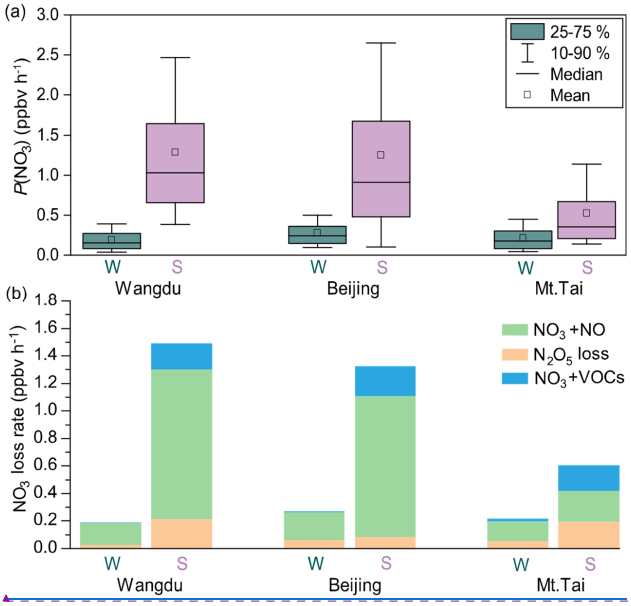

Formatted: Font color: Red
Formatted: Font: Italic
Formatted: Font color: Red
Formatted: Font color: Red
Formatted: Font color: Red
Formatted: Font: Times New Roman
Formatted: Centered

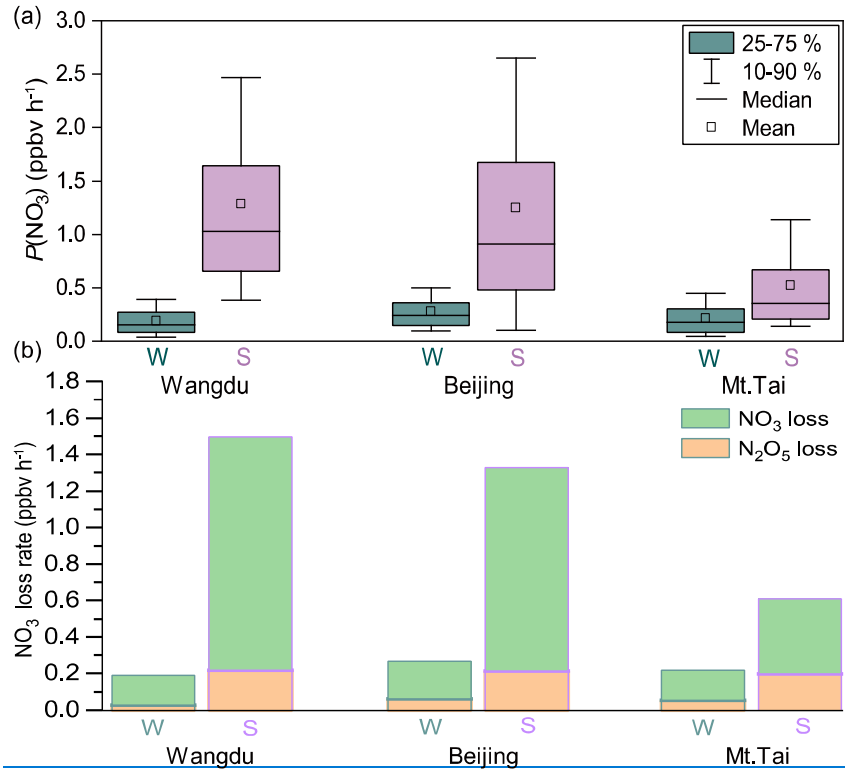

Figure 5–4. Comparison of $P(NO_3)$ and loss pathways of NO_3 during the winter and summer observations over the NCP. W and S are abbreviations for winter and summer, respectively.

The thermal decomposition of N_2O_5 was suppressed in winter and resulted in high ratios of N_2O_5/NO_3 (Fig. 6-5a; up to approximately 1000), which favored N_2O_5 loss over NO_3 loss. However, the $\gamma(N_2O_5)$ in winter was systematically lower than that in summer (Fig. 6-5b), which indicated slower N_2O_5 loss in winter. A previous field study in winter Beijing also reported small values of $\gamma(N_2O_5)$, ranging < 0.001 to 0.02 (Wang et al., 2020). This result differs from previous laboratory studies, which reported larger $\gamma(N_2O_5)$ on $(NH_4)_2SO_4$ aerosols at lower temperatures (Hallquist et al., 2003; Griffiths and Anthony Cox, 2009). It is possible that other factors, such as RH and aerosol composition (aside from $(NH_4)_2SO_4$), had a large influence on $\gamma(N_2O_5)$. The limited number (2–4) of $\gamma(N_2O_5)$ values obtained in each winter campaign (Table S6-4) may have also caused a bias in the estimation of the overall $\gamma(N_2O_5)$. The opposite effects – a higher N_2O_5/NO_3 ratio and lower $\gamma(N_2O_5)$ in winter – offset each other in Wangdu (Fig. 6-4b) but favored N_2O_5 loss in Beijing and NO_3 loss at Mt. Tai compared with those in the respective summer campaigns. The higher concentrations of $ClNO_2$ at Mt.

Formatted: Font color: Red

Formatted: Font color: Red

Formatted: Font color: Red

Formatted: Font color: Red

Formatted: Font color: Red

Tai during the winter campaigns may be attributable to higher φ($ClNO_2$) values in Mt. Tai (Fig. 6~~5~~c).

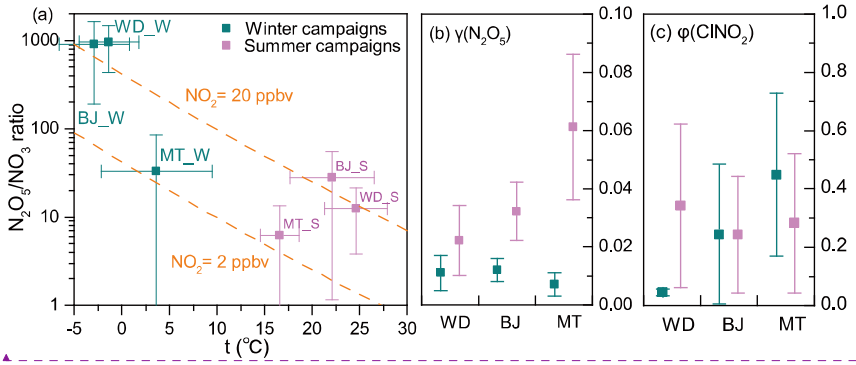

Figure 6~~5~~. Comparison of the **(a)** N_2O_5/NO_3 ratio, **(b)** γ(N_2O_5), and **(c)** φ($ClNO_2$) during the winter and summer campaigns. Square dots and error bars indicate the average values and standard deviations, respectively.

3.3 Daytime peaks in $ClNO_2$ concentrations

In the winter campaigns, high concentrations of $ClNO_2$ were sustained after sunrise. Distinct peaks in $ClNO_2$ concentrations were observed on 3–4 days in each campaign, as shown in Fig. 7 displaying one case at each site~~6~~. Other daytime cases from the three sites are shown in Fig. S1~~19~~–13~~11~~. The validity of the daytime peaks was checked by performing isotopic analysis of $ClNO_2$, background detection, and onsite calibration. ~~We also checked the signal of primary ions (I⁻ and IH_2O^-) and found no abnormal changes when $ClNO_2$ concentrations showed daytime peaks.~~ The signals of $I^{35}ClNO_2^-$ and $I^{37}ClNO_2^-$ were well correlated (R^2 > 0.99) during daytime peaks in $ClNO_2$ concentrations (Fig. S3a–c) and calibrations (Fig. S3d–f). The ratio of $I^{37}ClNO_2^-$ to $I^{35}ClNO_2^-$ (0.32–0.35) was consistent with the natural isotopic ratio of ^{37}Cl to ^{35}Cl. The background signals of $ClNO_2$ were checked when its daytime peaks in concentrations were observed, and no increase in the background was found. We also checked the signal of primary ions (~~I⁻ and~~ IH_2O^-) and found no abnormal changes when $ClNO_2$ concentrations showed daytime peaks. These results confirmed that the daytime peaks in $ClNO_2$ concentrations were real atmospheric phenomena.

The daytime-$ClNO_2$ episodes usually occurred from 10:00 to 11:00 LT at each site. The highest daytime mixing ratio of $ClNO_2$ was 1.3 ppbv (5-minute average) observed at 11:30 on 28 December 2017 in Wangdu. In comparison, the daytime $ClNO_2$ concentration observed in the previous summer study at Wangdu (Tham et al., 2016) reached a maximum in the early morning (08:00 LT) and declined to several pptv at 11:00 am. Attenuated solar radiation was observed during the days with daytime peaks in $ClNO_2$ concentrations. For example, the daily maximum rates of jNO_2 (1-minute average) for the Wangdu case shown in Fig. 7~~6~~a (2.5×10^{-3} s^{-1}) was significantly lower

Formatted: Font color: Red
Formatted: Font: Times New Roman
Formatted: Font: Times New Roman
Formatted: Font color: Red
Formatted: Font color: Red
Formatted: Font color: Red
Formatted: Font color: Red

than the highest rate observed during this campaign (6.0×10^{-3} s^{-1}). The attenuated solar radiation reduced the photolysis of $ClNO_2$, which allowed it to persist for a longer period during the day. The chemical data showed contrasting features during the daytime peaks in $ClNO_2$ concentrations at the three sites. At Wangdu, $ClNO_2$ concentrations showed a sharp peak while the concentrations of other pollutants decreased (Fig. 7~~6~~a); in Beijing, the daytime peak in $ClNO_2$ concentrations appeared with little simultaneous change in the NO_3^-, NO_x, and O_3 levels after sunrise (Fig. S12~~0~~a). In two cases, daytime peaks of $ClNO_2$ concentrations at Mt. Tai (Fig. 7~~6~~c and Fig. S13~~1~~c) occurred together with significant increases in NO_3^-, NO_x, and $PM_{2.5}$ levels, whereas O_3 concentrations decreased after sunrise and resumed its previous levels.

The daytime peaks in $ClNO_2$ concentrations were likely caused by the transport of air masses to the respective sites. In situ production of $ClNO_2$ was limited during the days on which significant daytime $ClNO_2$ occurred, because the mixing ratios of N_2O_5 were near the detection limit of the instrument (several pptv). The photochemical lifetime of $ClNO_2$ at 10:00 am LT was estimated to be 1 – 2 h, based on the inverse of $j$$ClNO_2$, which allowed the transport of $ClNO_2$ produced elsewhere to the observation sites. As daytime peaks in $ClNO_2$ concentrations appeared at both the ground and mountain sites, the high-$ClNO_2$ region may exist in the residual layer above the nocturnal mixing layers. At sunrise, $ClNO_2$-rich air masses may be transported downward to the ground sites (Wangdu and Beijing) and upward to the mountain-top site (Mt. Tai). The downward transport of $ClNO_2$ at Wangdu in summer has been illustrated by Tham et al. (2016), and the upward transport to the top of Mt. Tai has also been implicated by the increasing daytime concentrations of O_3 and other pollutants (e.g., Gao et al., 2005; Zhou et al., 2009; Jiang et al., 2020). Measurements in the residual layers are needed to further investigate the transport of $ClNO_2$ within the entire boundary layer.

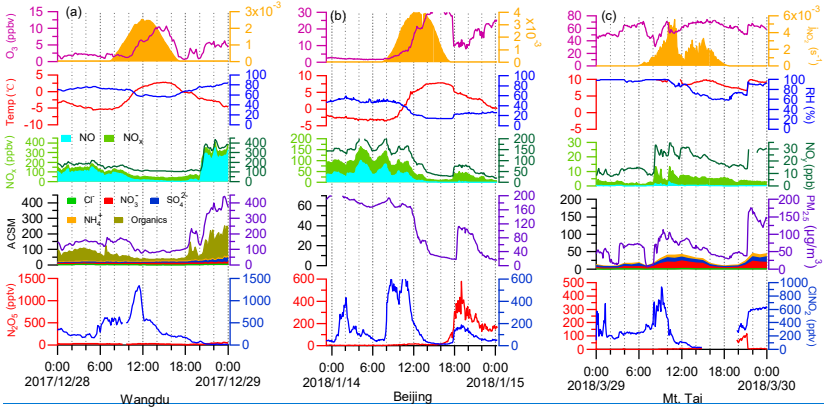

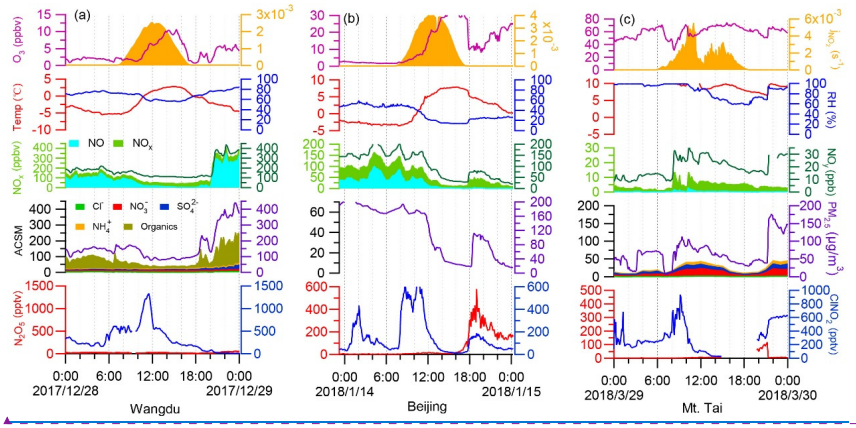

Figure 76. Examples of daytime peaks of $ClNO_2$ levels observed at **(a)** Wangdu, **(b)** Beijing, and **(c)** Mt. Tai in the winter campaigns. These examples show the highest levels of daytime $ClNO_2$ at each site. The ionic composition of aerosols was not available on 14 January 2018, owing to an instrument problem.

3.4 Impact of daytime $ClNO_2$ on atmospheric oxidation capacity

We used the box model (Section 2.5) to show the impact of $ClNO_2$ on photochemical oxidation at the three sites (Fig. 76a–c). In campaign-averaged conditions, the impact of $ClNO_2$ was minor, owing to the low daytime concentrations of $ClNO_2$. The daytime-averaged $P(Cl)$ (06:00–18:00 LT) from $ClNO_2$ photolysis was in the range of 0.03–0.06 ppbv h^{-1}, with the peak values of 0.07–0.12 ppbv h^{-1}, and the photolysis of $ClNO_2$ enhanced the daytime RO_x concentrations by 1.3–3.8 % and net O_3 production by 1.3–6.2 % at the three sites (figures not shown). Such impacts were lower than those during summer at Wangdu (Tham et al., 2016).

However, the impact of $ClNO_2$ increased considerably in the cases of daytime-peak concentrations, as shown in Fig. 87. The daytime-averaged $P(Cl)$ values from $ClNO_2$ photolysis were 0.15 ± 0.13 (maximum of 0.46), 0.11 ± 0.09 (maximum of 0.32), and 0.19 ± 0.20 (maximum of 0.74) ppbv h^{-1} at Wangdu, Beijing, and Mt. Tai, respectively (Fig. 87a–c). The winter $P(Cl)$ peak in Wangdu (Fig. 87a, 0.46 ppbv h^{-1}) was twice the summer average value (0.24 ppbv h^{-1}) (Tham et al., 2016). The P(Cl) during the daytime peaks of $ClNO_2$ in this study is significantly higher than that in Riedel et al. (2012) (maximum ~0.08 ppbv h^{-1}) but slightly lower than that in Haskins et al. (2019) (maximum ~1.3 ppbv h^{-1}). $P(Cl)$ from other sources (e.g., the HCl + OH reaction) was minor (8.8–14.5 %) during these cases. The relative importance of $ClNO_2$ in primary radical production varied among these sites. $ClNO_2$ had a minor contribution in Beijing but became increasingly important in Wangdu and Mt. Tai (Fig. 87b, c). HONO photolysis was the most important source of OH at the two ground sites, whereas O_3 was also important at Mt. Tai.

Formatted: Font: Times New Roman
Formatted: Font color: Red
Formatted: Font color: Red
Formatted: Font color: Red
Formatted: Font color: Red
Formatted: Font color: Red
Formatted: Font color: Red
Formatted: Subscript
Formatted: Font color: Red

The liberated Cl (mostly from $ClNO_2$ photolysis) accounted for 28.5–57.7 % of the daytime (06:00–18:00 LT) oxidation of alkanes, 6.1–13.7 % of that of alkenes, 5.3–14.2 % of that of aromatics, and 4.6–6.0 % of that of aldehydes in the cases of high levels of daytime $ClNO_2$. The Cl + VOCs reactions enhanced the production of OH, HO_2, and RO_2 by up to 15–22 %, 24–31 %, and 36–52 %, respectively (Fig. 87d–f). The photolysis of $ClNO_2$ increased the daytime net O_3 production by 5.4 ppbv (18 %), 2.8 ppbv (17 %), and 2.6 ppbv (13 %) at Wangdu, Beijing, and Mt. Tai, respectively (Fig. 87g–i). These results indicate the considerable impact of daytime $ClNO_2$ on the atmospheric oxidative capacity and production of secondary pollutants.

The impact of Cl in the NCP is likely larger than the result shown above. Our model calculations considered photolysis of $ClNO_2$ (and HCl + OH) as the source of Cl, but not other photolabile Cl-containing gases. However, in the Wangdu field campaign, we frequently observed elevated daytime concentrations of bromine chloride (BrCl) and molecular chlorine (Cl_2), which dominated the Cl production (Peng et al., 2020). In addition, our $ClNO_2$ measurements were conducted at polluted ground-level sites and at a high mountain site (1534 m a.s.l.), which are not in the nocturnal residual layer where strong $ClNO_2$ production is expected to occur (Zhang et al., 2017). It is thus highly desirable to measure $ClNO_2$ in the residual layer in future studies to comprehensively assess the role of $ClNO_2$ in the lower part of the atmosphere.

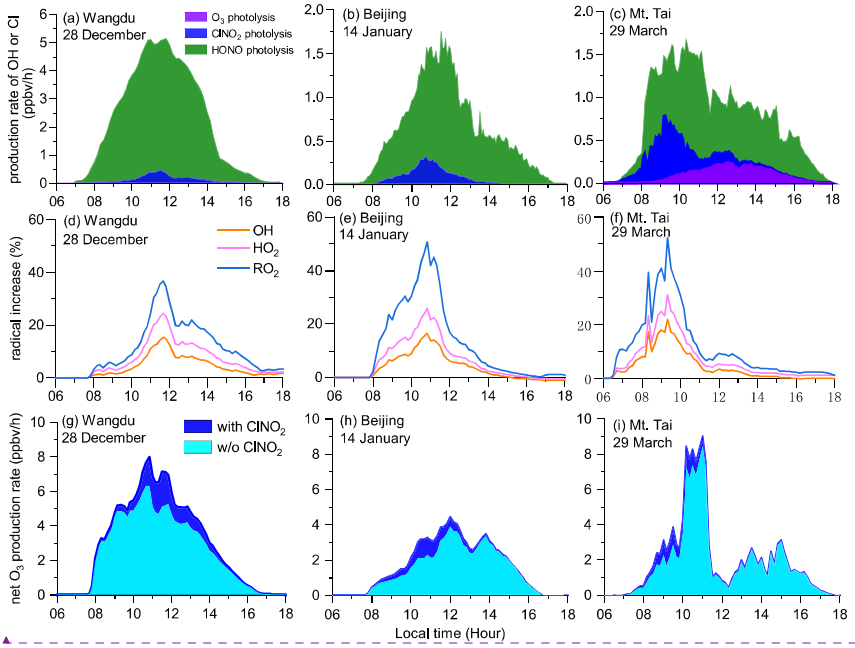

Figure 87. The impact of $ClNO_2$ photolysis on atmospheric oxidation during daytime-$ClNO_2$ episodes: **(a)** primary radical production from the photolysis of O_3, $ClNO_2$, and HONO; **(b)** percentage increase in OH, HO_2, and RO_2 due to $ClNO_2$ photolysis (Section

Formatted: Font color: Red

Formatted: Font color: Red

Formatted: Font: Times New Roman

Formatted: Font color: Red

2.5); and **(c)** enhancement of net O_3 production rates due to $ClNO_2$ photolysis.

4. Summary and conclusions

Observations of $ClNO_2$ and related species were conducted at urban, polluted rural, and polluted lower tropospheric ~~mountain top~~ sites in the winter of 2017 – 2018 in the NCP, which suffers from severe winter haze pollution. The winter measurements showed lower concentrations of $ClNO_2$ compared with those in previous summer observations. The campaign averaged NO_3 loss via reaction with NO at night dominated over the N_2O_5 loss at all the sites due to high NO concentrations, and in situ $ClNO_2$ formation was generally insignificant. However, high levels of daytime $ClNO_2$ (exceeding 1 ppbv) were observed at the three sites. We ~~suggest~~ suggest that $ClNO_2$ was efficiently produced in the nocturnal residual layer and was transported to ground-level and high-elevation sites. The daytime concentrations of $ClNO_2$ had great effects on the production of Cl, RO_x, and O_3. ~~These results represent polluted regions affected by fresh NO_x/SO_2 emissions, which is different from that in the clean troposphere or areas with more aged air masses.~~ Vertical measurements of the concentrations of $ClNO_2$ and related compounds are needed to better understand the distribution and impact of these species in the lower ~~part of the~~ troposphere. Compared to the previous studies in the clean troposphere or in more aged air masses, our results provide new insights into $ClNO_2$ formation in the region affected by fresh and intense anthropogenic emissions.

Formatted: Font color: Red

Formatted: Font color: Red

Formatted: Font color: Red

Formatted: Subscript

Data availability.

The datasets described in this study is available by contacting the corresponding author (cetwang@polyu.edu.hk).

Author contributions.

TW designed this study. JC, YM, LX, JG, and HL provided field measurement sites. MX, XP, and WW conducted the CIMS measurements. CY, ZW, YJT, HC, CZ, PL, and XW provided supporting data. XP and WW performed the box model simulation. MX analyzed and virtualized the research data. MX and TW wrote the manuscript with discussions and comments from all co-authors.

Competing interests.

The authors declare that they have no conflict of interest.

Acknowledgments.

The authors are grateful to Yujie Zhang, Fang Bi, Zhenhai Wu, and Xi Cheng for providing supporting data in Beijing. The authors acknowledge helpful discussions and opinions from Peng Wang, Xiao Fu, logistics support from Liwei Guan in Wangdu, and the meteorological observatory at Mt. Tai for providing experiment platforms.

Financial support.

This work was funded by National Natural Science Foundation of China (grant nos.

91544213, 91844301, and 41922051), the Hong Kong Research Grants Council (grant nos. T24-504/17-N and A-PolyU502/16), and National Key Research and Development Program of China (grant no. 2016YFC0200500).

References

Achtert, P., Birmili, W., Nowak, A., Wehner, B., Wiedensohler, A., Takegawa, N., Kondo, Y., Miyazaki, Y., Hu, M., and Zhu, T.: Hygroscopic growth of tropospheric particle number size distributions over the North China Plain, Journal of Geophysical Research: Atmospheres, 114, D00G07, 2009.

An, Z., Huang, R.-J., Zhang, R., Tie, X., Li, G., Cao, J., Zhou, W., Shi, Z., Han, Y., Gu, Z., and Ji, Y.: Severe haze in northern China: A synergy of anthropogenic emissions and atmospheric processes, Proceedings of the National Academy of Sciences, 116, 8657-8666, ~~10.1073/pnas.1900125116,~~ 2019.

Apodaca, R., Huff, D., and Simpson, W.: The role of ice in N_2O_5 heterogeneous hydrolysis at high latitudes, Atmospheric Chemistry and Physics, 8, 7451-7463, 2008.

Atkinson, R., and Arey, J.: Atmospheric degradation of volatile organic compounds, Chemical reviews, 103, 4605-4638, 2003.

Atkinson, R. and Arey, J.: Atmospheric degradation of volatile organic compounds, Chemical reviews, 103, 4605-4638, 2003.

Atkinson, R. and Lloyd, A. C.: Evaluation of kinetic and mechanistic data for modeling of photochemical smog, Journal of physical and chemical reference data, 13, 315-444, 1984.

Bannan, T. J., Booth, A. M., Bacak, A., Muller, J. B. A., Leather, K. E., Le Breton, M., Jones, B., Young, D., Coe, H., Allan, J., Visser, S., Slowik, J. G., Furger, M., Prévôt, A. S. H., Lee, J., Dunmore, R. E., Hopkins, J. R., Hamilton, J. F., Lewis, A. C., Whalley, L. K., Sharp, T., Stone, D., Heard, D. E., Fleming, Z. L., Leigh, R., Shallcross, D. E., and Percival, C. J.: The first UK measurements of nitryl chloride using a chemical ionization mass spectrometer in central London in the summer of 2012, and an investigation of the role of Cl atom oxidation, Journal of Geophysical Research: Atmospheres, 120, 5638-5657, ~~10.1002/2014jd022629,~~ 2015.

Bannan, T. J., Khan, M. A. H., Le Breton, M., Priestley, M., Worrall, S. D., Bacak, A., Marsden, N. A., Lowe, D., Pitt, J., and Allen, G.: A large source of atomic chlorine from $ClNO_2$ photolysis at a UK landfill site, Geophysical Research Letters, 46, 8508-8516, 2019.

Behnke, W., George, C., Scheer, V., and Zetzsch, C.: Production and decay of $ClNO_2$ from the reaction of gaseous N_2O_5 with NaCl solution: Bulk and aerosol experiments, Journal of Geophysical Research: Atmospheres, 102, 3795-3804, 1997.

Bertram, T., and Thornton, J.: Toward a general parameterization of N_2O_5 reactivity on aqueous particles: the competing effects of particle liquid water, nitrate and chloride, Atmospheric Chemistry and Physics, 9, 8351-8363, 2009.

Bertram, T. H., Thornton, J. A., Riedel, T. P., Middlebrook, A. M., Bahreini, R., Bates, T. S., Quinn, P. K., and Coffman, D. J.: Direct observations of N_2O_5 reactivity on ambient aerosol particles, Geophysical Research Letters, 36, L19803, 2009.

Breton, M. L., Hallquist, Å. M., Pathak, R. K., Simpson, D., Wang, Y., Johansson, J.,

Formatted: Font: (Default) Times New Roman, 12 pt

Formatted: Font: (Default) Times New Roman, 12 pt

Formatted: Font: 20 pt

Zheng, J., Yang, Y., Shang, D., and Wang, H.: Chlorine oxidation of VOCs at a semi-rural site in Beijing: significant chlorine liberation from $ClNO_2$ and subsequent gas-and particle-phase Cl–VOC production, Atmospheric Chemistry and Physics, 18, 13013-13030, 2018.

Brown, S., Ryerson, T., Wollny, A., Brock, C., Peltier, R., Sullivan, A., Weber, R., Dube, W., Trainer, M., and Meagher, J.: Variability in nocturnal nitrogen oxide processing and its role in regional air quality, Science, 311, 67-70, 2006.

Brown, S. S., Stark, H., Ryerson, T. B., Williams, E. J., Nicks, D. K., Trainer, M., Fehsenfeld, F. C., and Ravishankara, A.: Nitrogen oxides in the nocturnal boundary layer: Simultaneous in situ measurements of NO_3, N_2O_5, NO_2, NO, and O_3, Journal of Geophysical Research: Atmospheres, 108, 4299, 2003.

Brown, S. S., Dubé, W. P., Osthoff, H. D., Stutz, J., Ryerson, T. B., Wollny, A. G., Brock, C. A., Warneke, C., De Gouw, J. A., and Atlas, E.: Vertical profiles in NO_3 and N_2O_5 measured from an aircraft: Results from the NOAA P-3 and surface platforms during the New England Air Quality Study 2004, Journal of Geophysical Research: Atmospheres, 112, D22304, 2007.

Burkholder, J., Sander, S., Abbatt, J., Barker, J., Huie, R., Kolb, C., Kurylo, M., Orkin, V., Wilmouth, D., and Wine, P.: Chemical kinetics and photochemical data for use in atmospheric studies: evaluation number 18, Pasadena, CA: Jet Propulsion Laboratory, National Aeronautics and Space, 2015.

Chang, W. L., Bhave, P. V., Brown, S. S., Riemer, N., Stutz, J., and Dabdub, D.: Heterogeneous atmospheric chemistry, ambient measurements, and model calculations of N_2O_5: A review, Aerosol Science and Technology, 45, 665-695, 2011.

Crowley, J., Thieser, J., Tang, M., Schuster, G., Bozem, H., Beygi, Z. H., Fischer, H., Diesch, J., Drewnick, F., and Borrmann, S.: Variable lifetimes and loss mechanisms for NO_3 and N_2O_5 during the DOMINO campaign: contrasts between marine, urban and continental air, Atmospheric Chemistry and Physics, 11, 10853-10870, 2011.

DeMore, W. B., Sander, S. P., Golden, D., Hampson, R. F., Kurylo, M. J., Howard, C. J., Ravishankara, A., Kolb, C., and Molina, M.: Chemical Kinetics and Photochemical Data for Use in Stratospheric Modeling. Evaluation No. 12, 1997.

Edwards, P. M., Young, C. J., Aikin, K., deGouw, J., Dubé, W. P., Geiger, F., Gilman, J., Helmig, D., Holloway, J. S., Kercher, J., Lerner, B., Martin, R., McLaren, R., Parrish, D. D., Peischl, J., Roberts, J. M., Ryerson, T. B., Thornton, J., Warneke, C., Williams, E. J., and Brown, S. S.: Ozone photochemistry in an oil and natural gas extraction region during winter: simulations of a snow-free season in the Uintah Basin, Utah, Atmospheric Chemistry and Physics~~Atmos. Chem. Phys.~~, 13, 8955–8971, ~~https://doi.org/10.5194/acp-13-8955-2013,~~ 2013.

Eger, P., Friedrich, N., Schuladen, J., Shenolikar, J., Fischer, H., Tadic, I., Harder, H., Martinez, M., Rohloff, R., Tauer, S., Drewnick, F., Fachinger, F., Brooks, J., Darbyshire, E., Sciare, J., Pikridas, M., Lelieveld, J., and Crowley, J.: Shipborne measurements of $ClNO_2$ in the Mediterranean Sea and around the Arabian Peninsula during summer, Atmospheric Chemistry and Physics, 19, 12121-12140, ~~10.5194/acp-19-12121-2019,~~ 2019.

Formatted: Font: (Default) Times New Roman, 12 pt

Formatted: Font color: Auto

Faxon, C., Bean, J., and Ruiz, L.: Inland Concentrations of Cl_2 and $ClNO_2$ in Southeast Texas suggest chlorine chemistry significantly contributes to atmospheric reactivity, Atmosphere, 6, 1487-1506, 2015.

Finlayson-Pitts, B., Ezell, M., and Pitts, J.: Formation of chemically active chlorine compounds by reactions of atmospheric NaCl particles with gaseous N_2O_5 and $ClONO_2$, Nature, 337, 241-244, 1989.

Fu, X., Wang, T., Wang, S., Zhang, L., Cai, S., Xing, J., and Hao, J.: Anthropogenic emissions of hydrogen chloride and fine particulate chloride in China, Environmental Science & Technology, 52, 1644-1654, 2018.

Fu, X., Wang, T., Gao, J., Wang, P., Liu, Y., Wang, S., Zhao, B., and Xue, L.: Persistent Heavy Winter Nitrate Pollution Driven by Increased Photochemical Oxidants in Northern China, Environmental Science & Technology, 54, 3881-3889, 2020.

Gao, J., Wang, T., Ding, A., and Liu, C.: Observational study of ozone and carbon monoxide at the summit of mount Tai (1534 m asl) in central-eastern China, Atmospheric Environment, 39, 4779-4791, 2005.

Griffiths, P. T., and Anthony Cox, R.: Temperature dependence of heterogeneous uptake of N_2O_5 by ammonium sulfate aerosol, Atmospheric Science Letters, 10, 159-163, ~~10.1002/asl.225,~~ 2009.

Gu, Y., Li, Q., Wei, D., Gao, L., Tan, L., Su, G., Liu, G., Liu, W., Li, C., and Wang, Q.: Emission characteristics of 99 NMVOCs in different seasonal days and the relationship with air quality parameters in Beijing, China, Ecotoxicology and environmental safety, 169, 797-806, 2019.

Hallquist, M., Stewart, D. J., Stephenson, S. K., and Cox, R. A.: Hydrolysis of N_2O_5 on sub-micron sulfate aerosols, Physical Chemistry Chemical Physics, 5, 3453-3463, 2003.

Haskins, J. D., Jaegl~~é~~é, L., Shah, V., Lee, B. H., Lopez-Hilfiker, F. D., Campuzano-Jost, P., Schroder, J. C., Day, D. A., Guo, H., and Sullivan, A. P.: Wintertime Gas-Particle Partitioning and Speciation of Inorganic Chlorine in the Lower Troposphere Over the Northeast United States and Coastal Ocean, Journal of Geophysical Research: Atmospheres, 123, 12,897-812,916, 2018.

Haskins, J., Lopez-Hilfiker, F., Lee, B., Shah, V., Wolfe, G., DiGangi, J., Fibiger, D., McDuffie, E., Veres, P., and Schroder, J.: Anthropogenic control over wintertime oxidation of atmospheric pollutants, Geophysical Research Letters, 46, 14826-14835, 2019.

Jenkin, M., Young, J., and Rickard, A.: The MCM v3. 3.1 degradation scheme for isoprene, Atmospheric Chemistry and Physics, 15, 11433, 2015.

Jeong, D., Seco, R., Gu, D., Lee, Y., Nault, B. A., Knote, C. J., McGee, T., Sullivan, J. T., Jimenez, J. L., Campuzano-Jost, P., Blake, D. R., Sanchez, D., Guenther, A. B., Tanner, D., Huey, L. G., Long, R., Anderson, B. E., Hall, S. R., Ullmann, K., Shin, H., Herndon, S. C., Lee, Y., Kim, D., Ahn, J., and Kim, S.: Integration of airborne and ground observations of nitryl chloride in the Seoul metropolitan area and the implications on regional oxidation capacity during KORUS-AQ 2016, Atmospheric

Formatted: Font: (Default) Times New Roman, 12 pt

Formatted: Font: (Default) Times New Roman, 12 pt, Subscript

Formatted: Font: (Default) Times New Roman, 12 pt

Formatted: Font: (Default) Times New Roman, 12 pt, Subscript

Formatted: Font: (Default) Times New Roman, 12 pt

Formatted: Font color: Auto

Formatted: Font color: Red

Formatted: Font: (Default) Times New Roman, 12 pt

Chemistry and PhysicsAtmos. Chem. Phys., 19, 12779-12795, 10.5194/acp-19-12779-2019, 2019.

Kenagy, H. S., Sparks, T. L., Ebben, C. J., Wooldrige, P. J., Lopez-Hilfiker, F. D., Lee, B. H., Thornton, J. A., McDuffie, E. E., Fibiger, D. L., and Brown, S. S.: NO_x Lifetime and NO_y Partitioning During WINTER, Journal of Geophysical Research: Atmospheres, 123, 17, 2018.

Lewis, E. R.: An examination of Köhler theory resulting in an accurate expression for the equilibrium radius ratio of a hygroscopic aerosol particle valid up to and including relative humidity 100%, Journal of Geophysical Research: Atmospheres, 113, D03205, 2008.

Liu, X., Qu, H., Huey, L. G., Wang, Y., Sjostedt, S., Zeng, L., Lu, K., Wu, Y., Hu, M., and Shao, M.: High levels of daytime molecular chlorine and nitryl chloride at a rural site on the North China Plain, Environmental science & technology, 51, 9588-9595, 2017.

McCulloch, A., Aucott, M. L., Benkovitz, C. M., Graedel, T. E., Kleiman, G., Midgley, P. M., and Li, Y. F.: Global emissions of hydrogen chloride and chloromethane from coal combustion, incineration and industrial activities: Reactive Chlorine Emissions Inventory, Journal of Geophysical Research: Atmospheres, 104, 8391-8403, 1999.

McDuffie, E. E., Womack, C. C., Fibiger, D. L., Dube, W. P., Franchin, A., Middlebrook, A. M., Goldberger, L., Lee, B. H., Thornton, J. A., Moravek, A., Murphy, J. G., Baasandorj, M., and Brown, S. S.: On the contribution of nocturnal heterogeneous reactive nitrogen chemistry to particulate matter formation during wintertime pollution events in Northern Utah, Atmospheric Chemistry and PhysicsAtmos. Chem. Phys., 19, 9287-9308, 10.5194/acp-19-9287-2019, 2019.

McNamara, S. M., Raso, A. R., Wang, S., Thanekar, S., Boone, E. J., Kolesar, K. R., Peterson, P. K., Simpson, W. R., Fuentes, J. D., and Shepson, P. B.: Springtime Nitrogen Oxide-Influenced Chlorine Chemistry in the Coastal Arctic, Environmental science & technology, 53, 8057-8067, 2019.

Mielke, L., Stutz, J., Tsai, C., Hurlock, S., Roberts, J., Veres, P., Froyd, K., Hayes, P., Cubison, M., and Jimenez, J.: Heterogeneous formation of nitryl chloride and its role as a nocturnal NO_x reservoir species during CalNex-LA 2010, Journal of Geophysical Research: Atmospheres, 118, 10638-10652, 2013.

Mielke, L. H., Furgeson, A., and Osthoff, H. D.: Observation of $ClNO_2$ in a mid-continental urban environment, Environmental Science & Technology, 45, 8889-8896, 10.1021/es201955u, 2011.

Mielke, L. H., Furgeson, A., Odame-Ankrah, C. A., and Osthoff, H. D.: Ubiquity of $ClNO_2$ in the urban boundary layer of Calgary, Alberta, Canada, Canadian Journal of Chemistry, 94, 414-423, 2016.

Molina, M. J., and Rowland, F. S.: Stratospheric sink for chlorofluoromethanes: chlorine atom-catalysed destruction of ozone, Nature, 249, 810-812, 1974.

Nakayama, T., Ide, T., Taketani, F., Kawai, M., Takahashi, K., and Matsumi, Y.:

Formatted: Font: 16 pt

Formatted: Font color: Red

Formatted: Font: (Default) Times New Roman, 12 pt

Formatted: Font color: Auto

Formatted: Subscript

Nighttime measurements of ambient N_2O_5, NO_2, NO and O_3 in a sub-urban area, Toyokawa, Japan, Atmospheric Environment, 42, 1995-2006, 2008.

Osthoff, H. D., Roberts, J. M., Ravishankara, A. R., Williams, E. J., Lerner, B. M., Sommariva, R., Bates, T. S., Coffman, D., Quinn, P. K., Dibb, J. E., Stark, H., Burkholder, J. B., Talukdar, R. K., Meagher, J., Fehsenfeld, F. C., and Brown, S. S.: High levels of nitryl chloride in the polluted subtropical marine boundary layer, Nature Geoscience, 1, 324-328, ~~10.1038/ngeo177,~~ 2008.

Osthoff, H. D., Odame-Ankrah, C. A., Taha, Y. M., Tokarek, T. W., Schiller, C. L., Haga, D., Jones, K., and Vingarzan, R.: Low levels of nitryl chloride at ground level: nocturnal nitrogen oxides in the Lower Fraser Valley of British Columbia, Atmospheric Chemistry and Physics, 18, 6293-6315, 2018.

Peng, X., W. Wang, M. Xia, H. Chen, A. R. Ravishankara, Q. Li, A. Saiz-Lopez, P. Liu, F. Zhang, C. Zhang, L. Xue, X. Wang, C. George, J. Wang, Y. Mu, J. Chen, and T. Wang, An unexpected large continental source of reactive bromine and chlorine with significant impact on wintertime air quality, National Science Review, https://doi.org/10.1093/nsr/nwaa304, 2020

Phillips, G. J., Tang, M. J., Thieser, J., Brickwedde, B., Schuster, G., Bohn, B., Lelieveld, J., and Crowley, J. N.: Significant concentrations of nitryl chloride observed in rural continental Europe associated with the influence of sea salt chloride and anthropogenic emissions, Geophysical Research Letters, 39, L10811, ~~10.1029/2012gl051912~~, 2012.

Phillips, G. J., Thieser, J., Tang, M., Sobanski, N., Schuster, G., Fachinger, J., Drewnick, F., Borrmann, S., Bingemer, H., and Lelieveld, J.: Estimating N_2O_5 uptake coefficients using ambient measurements of NO_3, N_2O_5, $ClNO_2$ and particle-phase nitrate, Atmospheric Chemistry and Physics, 16, 13231-13249, 2016.

Priestley, M., Breton, M. l., Bannan, T. J., Worrall, S. D., Bacak, A., Smedley, A. R., Reyes-Villegas, E., Mehra, A., Allan, J., and Webb, A. R.: Observations of organic and inorganic chlorinated compounds and their contribution to chlorine radical concentrations in an urban environment in northern Europe during the wintertime, Atmospheric Chemistry and Physics, 18, 13481-13493, 2018.

Qian, X., Shen, H., and Chen, Z.: Characterizing summer and winter carbonyl compounds in Beijing atmosphere, Atmospheric Environment, 214, 116845, 2019.

Riedel, T., Wolfe, G., Danas, K., Gilman, J., Kuster, W., Bon, D., Vlasenko, A., Li, S.-M., Williams, E., and Lerner, B.: An MCM modeling study of nitryl chloride ($ClNO_2$) impacts on oxidation, ozone production and nitrogen oxide partitioning in polluted continental outflow, Atmospheric Chemistry and Physics, 14, 3789-3800, 2014.

Riedel, T. P., Bertram, T. H., Crisp, T. A., Williams, E. J., Lerner, B. M., Vlasenko, A., Li, S. M., Gilman, J., de Gouw, J., Bon, D. M., Wagner, N. L., Brown, S. S., and Thornton, J. A.: Nitryl chloride and molecular chlorine in the coastal marine boundary layer, Environmental Science & Technology, 46, 10463-10470, ~~10.1021/es204632r,~~ 2012.

Riedel, T. P., Wagner, N. L., Dubé, W. P., Middlebrook, A. M., Young, C. J., Öztürk, F., Bahreini, R., VandenBoer, T. C., Wolfe, D. E., and Williams, E. J.: Chlorine activation within urban or power plant plumes: Vertically resolved $ClNO_2$ and Cl_2 measurements

Formatted: Font: (Default) Times New Roman, 12 pt

Formatted: Font color: Auto

Formatted: Font: Times New Roman

Formatted: Font color: Red

from a tall tower in a polluted continental setting, Journal of Geophysical Research: Atmospheres, 118, 8702-8715, 2013.

Sandu, A., and Sander, R.: Simulating chemical systems in Fortran90 and Matlab with the Kinetic PreProcessor KPP-2.1, Atmospheric Chemistry and Physics, 6, 187-195, 2006.

Sommariva, R., Hollis, L. D., Sherwen, T., Baker, A. R., Ball, S. M., Bandy, B. J., Bell, T. G., Chowdhury, M. N., Cordell, R. L., and Evans, M. J.: Seasonal and geographical variability of nitryl chloride and its precursors in Northern Europe, Atmospheric Science Letters, 19, e844, 2018.

Tan, Z., Fuchs, H., Lu, K., Hofzumahaus, A., Bohn, B., Broch, S., Dong, H., Gomm, S., Häseler, R., and He, L.: Radical chemistry at a rural site (Wangdu) in the North China Plain: observation and model calculations of OH, HO_2 and RO_2 radicals, Atmospheric Chemistry and Physics, 17, 663-690, 2017.

~~Tan, Z., Rohrer, F., Lu, K., Ma, X., Bohn, B., Broch, S., Dong, H., Fuchs, H., Gkatzelis, G. I., and Hofzumahaus, A.: Wintertime photochemistry in Beijing: observations of RO_x radical concentrations in the North China Plain during the BEST-ONE campaign, Atmospheric Chemistry and Physics, 18, 12391-12411, 2018.~~

Tham, Y. J., Wang, Z., Li, Q., Yun, H., Wang, W., Wang, X., Xue, L., Lu, K., Ma, N., Bohn, B., Li, X., Kecorius, S., Größ, J., Shao, M., Wiedensohler, A., Zhang, Y., and Wang, T.: Significant concentrations of nitryl chloride sustained in the morning: investigations of the causes and impacts on ozone production in a polluted region of northern China, Atmospheric Chemistry and Physics, 16, 14959-14977~~, 10.5194/acp-16-14959-2016~~, 2016.

Thornton, J. A., Kercher, J. P., Riedel, T. P., Wagner, N. L., Cozic, J., Holloway, J. S., Dube, W. P., Wolfe, G. M., Quinn, P. K., Middlebrook, A. M., Alexander, B., and Brown, S. S.: A large atomic chlorine source inferred from mid-continental reactive nitrogen chemistry, Nature, 464, 271-274, ~~10.1038/nature08905,~~ 2010.

Wang, H., Lu, K., Chen, X., Zhu, Q., Chen, Q., Guo, S., Jiang, M., Li, X., Shang, D., and Tan, Z.: High N_2O_5 Concentrations Observed in Urban Beijing: Implications of a Large Nitrate Formation Pathway, Environmental Science & Technology Letters, 2017a.

Wang, H., Lu, K., Guo, S., Wu, Z., Shang, D., Tan, Z., Wang, Y., Breton, M. L., Zhu, W., and Lou, S.: Efficient N_2O_5 Uptake and NO_3 Oxidation in the Outflow of Urban Beijing, Atmospheric Chemistry and Physics, 18, 9705-9721, 2018.

Wang, H., Chen, X., Lu, K., Hu, R., Li, Z., Wang, H., Ma, X., Yang, X., Chen, S., and Dong, H.: NO_3 and N_2O_5 chemistry at a suburban site during the EXPLORE-YRD campaign in 2018, Atmospheric Environment, 224, 117180, 2019a.

Wang, H., Chen, X., Lu, K., Tan, Z., Ma, X., Wu, Z., Li, X., Liu, Y., Shang, D., and Wu, Y.: Wintertime N_2O_5 uptake coefficients over the North China Plain, 65, 765-774, Science Bulletin, 2020.

Wang, T., Tham, Y. J., Xue, L., Li, Q., Zha, Q., Wang, Z., Poon, S. C., Dubé, W. P., Blake, D. R., and Louie, P. K.: Observations of nitryl chloride and modeling its source and effect on ozone in the planetary boundary layer of southern China, Journal of Geophysical Research: Atmospheres, 121, 2476-2489, 2016.

Wang, X., Wang, H., Xue, L., Wang, T., Wang, L., Gu, R., Wang, W., Tham, Y. J., Wang,

Formatted: Font color: Red

Formatted: Font: (Default) Times New Roman, 12 pt, Font color: Red

Formatted: Font color: Red

Z., Yang, L., Chen, J., and Wang, W.: Observations of N_2O_5 and $ClNO_2$ at a polluted urban surface site in North China: High N_2O_5 uptake coefficients and low $ClNO_2$ product yields, Atmospheric Environment, 156, 125-134, 10.1016/j.atmosenv.2017.02.035, 2017b.

Wang, X., Jacob, D. J., Eastham, S. D., Sulprizio, M. P., Zhu, L., Chen, Q., Alexander, B., Sherwen, T., Evans, M. J., Lee, B. H., Haskins, J. D., Lopez-Hilfiker, F. D., Thornton, J. A., Huey, G. L., and Liao, H.: The role of chlorine in global tropospheric chemistry, Atmospheric Chemistry and Physics, 19, 3981-4003, 10.5194/acp-19-3981-2019, 2019b.

Wang, Z., Wang, W., Tham, Y. J., Li, Q., Wang, H., Wen, L., Wang, X., and Wang, T.: Fast heterogeneous N_2O_5 uptake and $ClNO_2$ production in power plant and industrial plumes observed in the nocturnal residual layer over the North China Plain, Atmospheric Chemistry and Physics, 17, 12361-12378, 2017c.

Wen, L., Xue, L., Wang, X., Xu, C., Chen, T., Yang, L., Wang, T., Zhang, Q., and Wang, W.: Summertime fine particulate nitrate pollution in the North China Plain: increasing trends, formation mechanisms and implications for control policy, Atmospheric Chemistry and Physics, 18, 11261-11275, 2018.

Wild, R. J., Edwards, P. M., Bates, T. S., Cohen, R. C., de Gouw, J. A., Dubé, W. P., Gilman, J. B., Holloway, J., Kercher, J., Koss, A. R., Lee, L., Lerner, B. M., McLaren, R., Quinn, P. K., Roberts, J. M., Stutz, J., Thornton, J. A., Veres, P. R., Warneke, C., Williams, E., Young, C. J., Yuan, B., Zarzana, K. J., and Brown, S. S.: Reactive nitrogen partitioning and its relationship to winter ozone events in Utah, Atmospheric Chemistry and Physics Atmos. Chem. Phys., 16, 573–583, https://doi.org/10.5194/acp-16-573-2016, 2016.

Xia, M., Wang, W., Wang, Z., Gao, J., Li, H., Liang, Y., Yu, C., Zhang, Y., Wang, P., Zhang, Y., Bi, F., Cheng, X., and Wang, T.: Heterogeneous Uptake of N_2O_5 in Sand Dust and Urban Aerosols Observed during the Dry Season in Beijing, Atmosphere, 10, 204, 2019.

Xia, M., Peng, X., Wang, W., Yu, C., Sun, P., Li, Y., Liu, Y., Xu, Z., Wang, Z., Xu, Z., Nie, W., Ding, A., and Wang, T.: Significant production of $ClNO_2$ and possible source of Cl_2 from N_2O_5 uptake at a suburban site in eastern China, Atmospheric Chemistry and Physics-, 20, 6147-6158, 10.5194/acp-20-6147-2020, 2020.

Xue, L., Saunders, S., Wang, T., Gao, R., Wang, X., Zhang, Q., and Wang, W.: Development of a chlorine chemistry module for the Master Chemical Mechanism, Geoscientific Model Development, 8, 3151-3162, 2015.

Yan, C., Tham, Y. J., Zha, Q., Wang, X., Xue, L., Dai, J., Wang, Z., and Wang, T.: Fast heterogeneous loss of N_2O_5 leads to significant nighttime NOx removal and nitrate aerosol formation at a coastal background environment of southern China, Science of The Total Environment, 677, 637-647, 2019.

Young, C., Washenfelder, R., Edwards, P., Parrish, D., Gilman, J., Kuster, W., Mielke, L., Osthoff, H., Tsai, C., and Pikelnaya, O.: Chlorine as a primary radical: evaluation of methods to understand its role in initiation of oxidative cycles, Atmospheric Chemistry and Physics, 14, 3427-3440, 2014.

Yun, H., Wang, T., Wang, W., Tham, Y. J., Li, Q., Wang, Z., and Poon, S.: Nighttime

NO_x loss and $ClNO_2$ formation in the residual layer of a polluted region: Insights from field measurements and an iterative box model, Science of the Total Environment, 622, 727-734, 2017.

Yun, H., Wang, W., Wang, T., Xia, M., Yu, C., Wang, Z., Poon, S. C. N., Yue, D., and Zhou, Y.: Nitrate formation from heterogeneous uptake of dinitrogen pentoxide during a severe winter haze in southern China, Atmospheric Chemistry and Physics, 18, 17515-17527~~, 10.5194/acp-18-17515-2018~~, 2018.

Zhang, F., Shang, X., Chen, H., Xie, G., Fu, Y., Wu, D., Sun, W., Liu, P., Zhang, C., Mu, Y., Zeng, L., Wan, M., Wang, Y., Xiao, H., Wang, G., and Chen, J.: Significant impact of coal combustion on VOCs emissions in winter in a North China rural site, Science of The Total Environment, 720, 137617~~, https://doi.org/10.1016/j.scitotenv.2020.137617~~, 2020.

Zhang, H., Li, H., Zhang, Q., Zhang, Y., Zhang, W., Wang, X., Bi, F., Chai, F., Gao, J., and Meng, L.: Atmospheric Volatile Organic Compounds in a Typical Urban Area of Beijing: Pollution Characterization, Health Risk Assessment and Source Apportionment, Atmosphere, 8, 61, 2017.

Zhou, W., Zhao, J., Ouyang, B., Mehra, A., Xu, W., Wang, Y., Bannan, T. J., Worrall, S. D., Priestley, M., and Bacak, A.: Production of N_2O_5 and $ClNO_2$ in summer in urban Beijing, China, Atmospheric Chemistry and Physics, 18, 11581-11597, 2018.

Zhou, Y., Wang, T., Gao, X., Xue, L., Wang, X., Wang, Z., Gao, J., Zhang, Q., and Wang, W.: Continuous observations of water-soluble ions in $PM_{2.5}$ at Mount Tai (1534 m a.s.l.) in central-eastern China, Journal of Atmospheric Chemistry, 64, 107-127, 2009.

Page 9: [1] Formatted XIA, Daniel [Student] 07/18/2021 12:20:00

Font: Times New Roman

Page 9: [1] Formatted XIA, Daniel [Student] 07/18/2021 12:20:00

Font: Times New Roman

Page 9: [1] Formatted XIA, Daniel [Student] 07/18/2021 12:20:00

Font: Times New Roman

Page 9: [1] Formatted XIA, Daniel [Student] 07/18/2021 12:20:00

Font: Times New Roman

Page 9: [2] Formatted XIA, Daniel [Student] 07/18/2021 12:20:00

Font: Times New Roman

Page 9: [2] Formatted XIA, Daniel [Student] 07/18/2021 12:20:00

Font: Times New Roman

Page 9: [2] Formatted XIA, Daniel [Student] 07/18/2021 12:20:00

Font: Times New Roman

Page 9: [2] Formatted XIA, Daniel [Student] 07/18/2021 12:20:00

Font: Times New Roman

Page 9: [2] Formatted XIA, Daniel [Student] 07/18/2021 12:20:00

Font: Times New Roman

Page 9: [2] Formatted XIA, Daniel [Student] 07/18/2021 12:20:00

Font: Times New Roman

Page 9: [3] Formatted XIA, Daniel [Student] 07/18/2021 12:28:00

Font: Times New Roman

Page 9: [3] Formatted XIA, Daniel [Student] 07/18/2021 12:28:00

Font: Times New Roman

Page 9: [3] Formatted XIA, Daniel [Student] 07/18/2021 12:28:00

Font: Times New Roman

Page 9: [3] Formatted XIA, Daniel [Student] 07/18/2021 12:28:00

Font: Times New Roman

Page 9: [3] Formatted XIA, Daniel [Student] 07/18/2021 12:28:00

Font: Times New Roman

Page 9: [3] Formatted XIA, Daniel [Student] 07/18/2021 12:28:00

Font: Times New Roman

Page 9: [3] Formatted XIA, Daniel [Student] 07/18/2021 12:28:00

Font: Times New Roman

Page 9: [3] Formatted XIA, Daniel [Student] 07/18/2021 12:28:00

Font: Times New Roman

Page 9: [3] Formatted XIA, Daniel [Student] 07/18/2021 12:28:00

Font: Times New Roman

Page 9: [3] Formatted XIA, Daniel [Student] 07/18/2021 12:28:00

Font: Times New Roman

Page 9: [3] Formatted XIA, Daniel [Student] 07/18/2021 12:28:00

Font: Times New Roman

Page 9: [3] Formatted XIA, Daniel [Student] 07/18/2021 12:28:00

Font: Times New Roman

Page 9: [4] Formatted XIA, Daniel [Student] 07/18/2021 12:28:00

Font: Times New Roman

Page 9: [4] Formatted XIA, Daniel [Student] 07/18/2021 12:28:00

Font: Times New Roman

Page 9: [5] Formatted XIA, Daniel [Student] 07/18/2021 12:20:00

Font color: Red

Page 9: [5] Formatted XIA, Daniel [Student] 07/18/2021 12:20:00

Font color: Red

Page 9: [5] Formatted XIA, Daniel [Student] 07/18/2021 12:20:00

Font color: Red

Page 9: [5] Formatted XIA, Daniel [Student] 07/18/2021 12:20:00

Font color: Red

Page 9: [5] Formatted XIA, Daniel [Student] 07/18/2021 12:20:00

Font color: Red

Page 9: [5] Formatted XIA, Daniel [Student] 07/18/2021 12:20:00

Font color: Red

Page 9: [5] Formatted XIA, Daniel [Student] 07/18/2021 12:20:00

Font color: Red

Page 9: [5] Formatted XIA, Daniel [Student] 07/18/2021 12:20:00

Font color: Red

Page 9: [5] Formatted XIA, Daniel [Student] 07/18/2021 12:20:00

Font color: Red

Page 9: [5] Formatted XIA, Daniel [Student] 07/18/2021 12:20:00

Font color: Red

Page 9: [5] Formatted XIA, Daniel [Student] 07/18/2021 12:20:00

Font color: Red

Page 9: [5] Formatted XIA, Daniel [Student] 07/18/2021 12:20:00

Font color: Red

Page 9: [5] Formatted XIA, Daniel [Student] 07/18/2021 12:20:00

Font color: Red

Page 9: [5] Formatted XIA, Daniel [Student] 07/18/2021 12:20:00

Font color: Red

Page 9: [5] Formatted XIA, Daniel [Student] 07/18/2021 12:20:00

Font color: Red

Page 9: [5] Formatted XIA, Daniel [Student] 07/18/2021 12:20:00

Font color: Red

Page 9: [5] Formatted XIA, Daniel [Student] 07/18/2021 12:20:00

Font color: Red

Page 9: [5] Formatted XIA, Daniel [Student] 07/18/2021 12:20:00

Font color: Red

Page 9: [5] Formatted XIA, Daniel [Student] 07/18/2021 12:20:00

Font color: Red

Page 9: [5] Formatted XIA, Daniel [Student] 07/18/2021 12:20:00

Font color: Red

Page 9: [5] Formatted XIA, Daniel [Student] 07/18/2021 12:20:00

Font color: Red

Page 9: [5] Formatted XIA, Daniel [Student] 07/18/2021 12:20:00

Font color: Red

Page 9: [5] Formatted XIA, Daniel [Student] 07/18/2021 12:20:00

Font color: Red

Page 9: [5] Formatted XIA, Daniel [Student] 07/18/2021 12:20:00

Font color: Red

Page 9: [5] Formatted XIA, Daniel [Student] 07/18/2021 12:20:00

Font color: Red

Page 9: [5] Formatted XIA, Daniel [Student] 07/18/2021 12:20:00

Font color: Red